Journal Pre-proofs

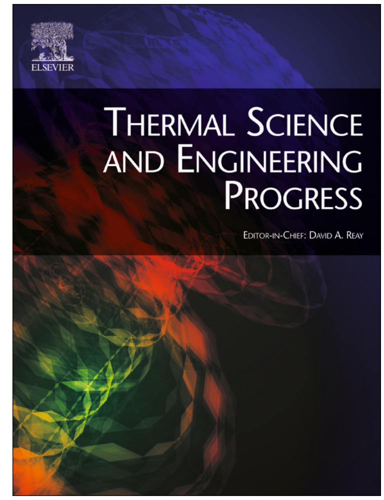


# Combination of $Co_3O_4$ deposited rGO hybrid nanofluids and longitudinal strip inserts: Thermal properties, heat transfer, friction factor, and thermal performance evaluations

L. Syam Sundar, Zafar Said, Bahaa Saleh, Manoj K. Singh, António C.M. Sousa

PII: S2451-9049(20)30215-8
DOI: https://doi.org/10.1016/j.tsep.2020.100695
Reference: TSEP 100695

To appear in: *Thermal Science and Engineering Progress*

Received Date: 29 June 2020
Revised Date: 19 August 2020
Accepted Date: 19 August 2020

Please cite this article as: L. Syam Sundar, Z. Said, B. Saleh, M.K. Singh, A.C.M. Sousa, Combination of $Co_3O_4$ deposited rGO hybrid nanofluids and longitudinal strip inserts: Thermal properties, heat transfer, friction factor, and thermal performance evaluations, *Thermal Science and Engineering Progress* (2020), doi: https://doi.org/10.1016/j.tsep.2020.100695

# Combination of $Co_3O_4$ deposited rGO hybrid nanofluids and longitudinal strip inserts: Thermal properties, heat transfer, friction factor, and thermal performance evaluations

**L. Syam Sundar[1,*], Zafar Said[2], Bahaa Saleh[3,4], Manoj K. Singh[5,*], António C.M. Sousa[1]**

[1]Centre for Mechanical Technology and Automation (TEMA–UA), Department of Mechanical Engineering, University of Aveiro, 3810-131 Aveiro, Portugal

[2]Department of Sustainable and Renewable Energy Engineering, University of Sharjah, United Arab Emirates

[3]Department of Mechanical Engineering, Taif University, Taif, Kingdom of Saudi Arabia

[4]Department of Mechanical Engineering, Assiut University, Assiut, Egypt

[5]Department of Physics – School of Engineering and Technology (SOET), Central University of Haryana (CHU), Mahendergarh 123031, Haryana, India

*Corresponding authors: sslingala@gmail.com (LSS), manojsingh@cuh.ac.in (MKS)

**Abstract**

The reduced-graphene oxide/cobalt oxide hybrid nanoparticles were prepared based on the *in-situ*/chemical co-precipitation technique, and they were analyzed by transmission electron microscope, x-ray diffraction, and magnetometer techniques. The hybrid nanofluids were prepared with particle loadings of 0.05%, 0.1%, and 0.2% by dispersing synthesized reduced-graphene oxide/cobalt oxide in distilled water and their physical properties were measured. The thermal performance of the nanofluids was studied, when they flow in the turbulent regime through a circular tube. The thermal performance was also evaluated when straight (longitudinal) strip inserts with aspect ratios of 1, 2, and 4, were used inside the circular. These straight strip inserts by increasing the flow turbulence intensity act as turbulators. Results indicate that with a dilution of 0.2% concentration of hybrid nanoparticles in water, the Nusselt number is enhanced by 25.65%, and it is further enhanced by 110.56% with a straight strip insert of aspect ratio 1. The use of hybrid nanofluids and straight strip inserts leads to a slight penalty in fluid friction. For 0.2% concentration of hybrid nanoparticles in water, the penalty in friction factor is 11%, and it is further increased to 69.8% with 0.2% particle loadings and a straight strip insert of aspect ratio1. Moreover, the thermal performance factor of hybrid nanofluids with and without straight strip inserts presents values higher than 1, which shows the benefit of the prepared hybrid nanofluids in a turbulent flow. A general form of regression equations are developed based on the experimental data.

**Keywords:** Thermal performance factor; hybrid nanofluids; longitudinal strip inserts; enhancement.

## 1. Introduction

In most of the thermal power plants and chemical industries, single-phase fluids (water, ethylene glycol, propylene glycol, and engine oil) are used as heat transfer fluids in heat exchangers. The performance improvement of these heat exchangers with the use of single-phase fluids tends to be a challenge; however, by using passive heat transfer enhancement techniques, the performance improvement is possible. The passive techniques include the replacement of single-phase fluids by high thermal conductivity fluids (nanofluids) and the insertion of flow turbulence promoters (turbulators).

The dilution of solid-nanometer sized particles in single-phase fluids is termed as nanofluids, which was developed by Choi [1], and reported an increased thermal conductivity of these nanofluids. Once the thermal conductivity of the fluid is increased, its heat transfer rate also increased because both are directly proportional. Several nanoparticles are available such as $Al_2O_3$, Cu, CuO, carbon-based, $Co_3O_4$, $Fe_3O_4$, $Fe_2O_3$, $SiO_2$, $TiO_2$, ZnO, etc., and by means of these nanoparticles based nanofluids the thermal conductivity is enhanced [2-9].

The particle thermal conductivity is also one of the influencing parameter on the nanofluids thermal conductivity. From the various nanoparticles, the carbon-based nanomaterials exhibit high thermal conductivity. Examples of carbon-based nanoparticles are CNT (carbon nanotubes), GO (graphene oxide), and ND (nanodiamond). From the carbon allotropes, the graphene material contains an increased thermal conductivity in the order of ~5000 W/m K and excellent electrical, mechanical and optical properties [10].

The exfoliated sheets contain one layer or few layers of carbon atoms like graphene; these sheets are known as graphene oxide (GO); it is a 2-dimensional structure. The removed, decorated oxygen-containing groups are known as reduced-graphene oxide. In other words, the reduced-GO (rGO) sheets are known as chemically modified graphene, which are also called as chemically modified graphene, functionalized graphene, chemically converted graphene, or reduced graphene [11], which, in particular, has a variety of applications, as an electrode in lithium rechargeable batteries [12], and energy storage devices [13]. Apart from these applications, the rGO based nanofluids have considerable potential as heat transfer fluids.

Sadeghinezhad et al. [14] studied the heat transfer coefficient for graphene oxide/water nanofluids flow in a tube, for 0.075% and 0.1% weight concentration of nanoparticles, they obtained heat transfer enhancement of 13% and 160%, respectively, and friction factor penalty of 0.4% and 14.6%, respectively. Esfahani et al. [15] also analyzed heat transfer coefficient and pressure drop of graphene oxide/water nanofluids flow in a tube and noticed enhanced heat transfer rates with the use of GO/water nanofluids. Ponangi et al. [16] considered 50:50% ethylene/water-mixture based graphene oxide nanofluids flow in a tube and for 0.03% volume concentration of nanofluid at a volume flow rate of 5 LPM, they obtained maximum effectiveness of 56.45% and 41.47% at temperatures of 40$^o$C and 50$^o$C, respectively.

As already mentioned, particle thermal conductivity to a great extent determines the thermal conductivity of the nanofluids. Changing the particle thermal conductivity is possible by manufacturing or synthesizing the nanoparticles by combining two or more nanoparticles, which, in this case, are known as composite or hybrid nanoparticles. Consequently, the nanofluids prepared using hybrid nanoparticles are known as hybrid nanofluids.

Relevant research work related to the thermal properties of various types of hybrid nanofluids is given in what follows. Soltani et al. [17] prepared tungsten oxide ($WO_3$) and MWCNTs/engine oil based hybrid nanofluids and studied the effect of particle loading and temperature on thermal conductivity. They obtained thermal conductivity enhancement of 19.89% for particle concentration of 0.6% and temperature of 60°C. Singh et al. [18] experimentally measured the thermal conductivity for GO-CuO/water hybrid nanofluids and compared it with that of CuO/water and GO/water nanofluids. For 0.3% weight percentage and temperature of 60°C, they observed that GO-CuO/water, CuO/water and GO/water nanofluids led to thermal conductivity enhancement, as compared to water data, of 30%, 12.4% and 51.6%, respectively. Sahoo and Kumar [19] prepared $Al_2O_3$-CuO-$TiO_2$/water ternary hybrid nanofluids and studied experimentally the viscosity for different values of temperature and concentration. For 0.1% volume fraction of $Al_2O_3$-$TiO_2$ and $Al_2O_3$-CuO hybrid nanofluids at a temperature of 45°C, they observed a viscosity increase, as compared to water, of 55.41% and 17.25%, respectively. Vallejo et al. [20] prepared silver/graphene nanoplatelet based 10:90% mixture of propylene glycol and water hybrid nanofluids and studied their optical, rheological and thermo-physical properties. They observed that the nanofluids present Newtonian behaviours and the viscosity increase, as compared to the base fluid data, is 9% for a 0.1 wt. % concentration of nanofluids.

Gupta et al. [21] investigated the stability and thermal conductivity of water based Ag/COOH-MWCNT, Cu/COOH-MWCNT, Fe/COOH-MWCNT and Zn/COOH-MWCNT hybrid nanofluids; increasing stability and thermal conductivity enhancement of the hybrid nanofluids was observed in the following order: Cu/COOH-MWCNT, Fe/COOH-MWCNT, Ag/COOH-MWCNT and Zn/COOH-MWCNT in distilled water. Wole-Osho et al. [22] prepared $Al_2O_3$-ZnO water hybrid nanofluids for different values of mixture ratio and studied experimentally their influence of specific heat and viscosity. For the 2:1 mixture ratio (particle loading of 1.67%), they obtained maximum viscosity penalty of 96.37% and specific heat decrease of 30.12% at a temperature of 25°C; they found that the 1:1 mixture ratio is the best for heat transfer applications. Sahoo [23] prepared water based $Al_2O_3$/CNT/Graphene ternary hybrid nanofluids and studied their heat transfer, pressure drop, irreversibility, entropy generation and exergy loss when they flow through a radiator. For the 3% volume concentration of ternary hybrid nanofluid, heat transfer, second law efficiency and irreversibility increase by 18.45%, 6.3% and 42.45%, respectively, as compared to water data. Pourrajab et al. [24] synthesized and prepared water based mesoporous silica modified with copper nanoparticles hybrid nanofluids and studied the influence on the thermal conductivity of particle concentration by weight in the range from 0.019% to 0.075% and of temperature in the range from 25 to 50$^{o}$C. They obtained higher thermal conductivity of hybrid nanofluids as concentration and temperature are increased, and their study proposes a thermal conductivity empirical correlation fitting their experimental data. Singh and Sarkar [25] conducted heat transfer experiments for $Al_2O_3$+MgO hybrid nanofluid flow in a double-pipe heat exchanger with the addition of tapered wire coil configurations of converging (C) type, diverging (D) type and converging-diverging (C-D) type forthe turbulent flow. For D-type, C-D type and C-type tapered wire coil inserts in the hybrid nanofluids, the observed Nusselt number enhancement is 84%, 71% and 47%, respectively, and friction factor penalty is 68%, 57% and 46%, respectively, compared to the use of water without inserts. Asadi et al. [26] studied the rheological behaviour and dynamic viscosity of the CuO-$TiO_2$/water hybrid nanofluid forthe particle volume concentration range from 0.1 to 1% and temperature range from 25 to 55$^{o}$C; they observed that hybrid nanofluids behave like Newtonian fluid and they noted maximum viscosity increase for the 1% volume concentration.

Sheikholeslami et al. [27] studied numerically the energy and entropy related to a solar unit, which uses three types of turbulators, twisted tape, barrier twisted tape and perforated barrier twisted tape, and the working fluid is a nanofluid. The nanomaterial is formulated using the mixture model and turbulence is described by the k-$\varepsilon$ model; they found that with the use of the twisted tape inserts, thermal entropy generation and pumping power increased by 8.88% and 3.17%, respectively. Later on, Sheikholeslami et al. [28] designed a novel energy storage device to work with the solar unit. Paraffin with melting point of 28ºC is used as the phase-change material (PCM) in the storage device. By adding nanoparticles to the PCM, its viscosity and thermal conductivity improved, which led to enhanced efficiency of the energy storage device; they also noticed that the use of nanoparticles resulted in an improvement of the solidification process by 21.4%.

Taherialekouhi et al. [29] studied the thermal conductivity of GO/$Al_2O_3$ hybrid nanofluids and, compared to water data, they observed thermal conductivity enhancement of 33.9% with 1% volume fraction of nanofluid for a temperature of 50°C. Afrand [30] examined the thermal conductivity of ethylene glycol by adding nanoparticles of f-MWCNTs and magnesium oxide (MgO) by varying the temperature from 25 to 50°C and the volume fraction from 0 to0.6%. They observed a thermal conductivity enhancement in of 21.3% for a temperature of 25°C and volume fraction of 0.6%. Said et al. [31] investigated carbon nanotubes/reduced graphene oxide based hybrid nanofluids and analyzed their thermophysical properties characteristics using fuzzy logic techniques. Gupta et al. [32] conducted research on the heat transfer of zinc ferrite/water hybrid nanofluids and they observed heat transfer coefficient augmentation of hybrid nanofluids, in addition, they proposed a new correlation. Nine et al. [33] prepared $Al_2O_3$-MWCNTs hybrid nanofluids to investigate the thermal conductivity in the volume concentrations range from 1 to 6% and they observed an increased thermal conductivity of the nanofluids. Kazemi et al. [34] prepared 30% graphene and 70% silicon water-based hybrid nanofluids and they studied viscosity for particle loading range from 0.05% to 1% and temperature range from 25 to 50°C and they observed that the nanofluids present a non-Newtonian pseudoplastic behaviour. Soltani and Akbari [35] studied the viscosity of MgO-MWCNT ethylene glycol based hybrid nanofluids. They noticed Newtonian behaviour for the range of solid volume fraction (0 to 1%) and temperature (30ºC to 60%) studied. They observed an increase of relative dynamic viscosity of 168% when the solid volume fraction varies from 0.1% to 1%. An increase in temperature leads to a reduction of dynamic viscosity.

Rahimi et al. [36] described the enhanced natural convection heat transfer based on the experimental and numerical study by considering 75:25% MWCNT-MgO/water hybrid nanofluids in a three dimensional enclosure at 2 vol. %. Mansour et al. [37] have noticed the experimental natural convection heat transfer of Cu-$Al_2O_3$-water hybrid nanofluids is good agreement with the theoretical data while the nanofluids flow in a square porous cavity. Tayebi et al. [38] proven the combined effect of internal heat generation and absorption of Cu-$Al_2O_3$/$H_2O$ based hybrid nanofluids significantly change the heat transfer and entropy generation in the annulus of double pipe heat exchanger. Saghir and Bayomy [39] have considered as 20:3% of microencapsulated phase change material and $Al_2O_3$ hybrid nanofluids as a heat storage material and observed a 6% improvement in heat removal factor.

Shin et al. [40] have studied the photo-thermal energy conversion performance of MWCNT/$Fe_3O_4$ hybrid nanofluid by using magnetic field. They observed photo-thermal energy conversion efficiency of 32.8% and 45.1% without and with external magnetic field at 0.2 wt. % of hybrid nanofluid. Goudarzi et al. [41] have studied the natural convective heat transfer coefficient, particle migration and Brownian motion of Ag-MgO/Water hybrid nanofluid in a sinusoidal enclosure and they observed Nusselt number enhancement of 11%. Urmi et al. [42] obtained the thermal conductivity enhancement of 40.86% by using 0.1 vol. % of 40% ethylene glycol based $TiO_2$- $Al_2O_3$ hybrid nanofluids at a temperature of 80°C. Boroomandpour et al. [43] have studied the thermal conductivity of multi-walled carbon Nanotubes-titania-zinc oxide/80:20% water-ethylene glycol hybrid nanofluds and observed a maximum thermal conductivity enhancement of 17.82% using MWCNT/Water-EG nanofluid at 0.4 vol. % and at a temperature of 50°C. Kadhim et al. [44] explained numerically the natural convection heat transfer of Cu-$Al_2O_3$/water hybrid nanofluids is better when compared to $Al_2O_3$/water nanofluids when they flow in enclosure with opposite wavy wall. Oliveira et al. [45] have obtained maximum thermal conductivity and viscosity enhancements of 6.92% and 21.21% for 0.1 vol. % of nanodiamond-silver/ethylene glycol hybrid nanofluids at a temperature of 10°C compared to base fluid. In the above mentioned works, the researchers have found better thermal conductivity and heat transfer rates with the use of hybrid nanofluids.

Several experimental studies have conducted for the graphene based nanocomposite nanofluids flowing in a horizontal tube, namely $SiO_2$-graphene-water [46], graphene wrapped MWCNTs-water, and MWCNTs-EG [47] and graphene oxide-silver [48], found higher heat transfer rates.

The graphene based cobalt oxide ($Co_3O_4$) nanocomposite nanofluids are interesting because they possess both high thermal conductivity (GO) and magnetic property ($Co_3O_4$). These GO/$Co_3O_4$ nanoparticles can be used in lithium-ion batteries [49,50], catalytic [51,52] and super-capacitor applications [53], in addition to these applications, the GO/$Co_3O_4$based nanofluids can be used as heat transfer fluids due to their high thermal conductivity [54].

Another passive heat transfer enhancement technique consists in the insertionof straight strips into the fluid flow path. Heish and Wen [55] first used the concept of straight strip inserts. Heish and Huang [56] used the concept of straight strip inserts for single-phase fluid in laminar regime, later on Liu [57] extended the work for turbulent flow. In another study, Sundar et al. [58] used the same concept of straight strip inserts for $Al_2O_3$ nanofluids turbulent flow in a circular tube. In addition, Sundar et al. [59, 60] applied the straight strip inserts concept to MWCNT/$Fe_3O_4$ and ND-Ni hybrid nanofluids turbulent flow in a circular tube. These authors noticed that the straight strip inserts led to further heat transfer coefficient augmentation with a relatively negligible fluid friction factor penalty.

The heat transfer and thermal performance benefits of cobalt oxide ($Co_3O_4$) nanoparticles decorated rGO hybrid nanomaterial based nanofluids data is not available in the literature. Hence, the current study aims to investigate experimentally the thermal performance benefits of rGO/$Co_3O_4$ hybrid nanomaterial based nanofluids turbulent flow in a plain horizontal tube. The experiments are conducted for different values of hybrid nanomaterial volume concentration (0.05%, 0.1%, and 0.2%) and Reynolds number (2000 to 20000). The obtained data is compared against values available from the open literature. The experiments are also conducted using the straight strip inserts. The friction factor is also analyzed for different nanomaterial loading (volume concentration), temperature, Reynolds number and aspect ratio of the straight strip inserts. The obtained data is compared against values available in the literature. The experimental data for Nusselt number and friction factor is regressed and for each one of these parameters a single form correlation is proposed.

## 2. Synthesis and characterization

### 2.1. Reduced graphene oxide (rGO) nanosheets

The method used is similar to that of Hummers [61] for the synthesis of reduced graphene oxide (rGO) nanosheets. The steps are as follows: (i) 2 g of graphite powder are dispersed in 70 ml of sulphuric acid (concentrated) and then are added 0.025 mole of $NaNO_3$, while the container is cooled with ice-water, (ii) then 0.039 moles of potassium permanganate are added to the above mixture and stirred for 20 minutes at a temperature of $0^oC$, (iii) the solution colour changes to green due the presence of oxidizing agent ($MnO^{3+}$), (iv) the solution is brought back to normal room temperature by adding water, (v) the solution is diluted by adding the water and then washed with 70 ml of hydrogen peroxide ($H_2O_2$) (30 wt.%) for 30 minutes, (v) the solution is centrifuged and washed several times with de-ionized water, (vi) the produced rGO is dried at a temperature of $60^oC$ in a vacuum oven for 12 hours, (vii) the dried rGO is dispersed in strong hydrochloric (HCl) acid for 48 hours. The steps were repeated for several times to prepare the required quantity of rGO nanosheets. Due to the concentrated hydrochloric acid, carboxyl (COOH) groups develop on the top surface of the rGO nanosheets, which is advantageous for the deposition of $Co_3O_4$ nanoparticles.

**2.2. $Co_3O_4$ deposition on rGO nanosheets**

The synthesis process is depicted in **Fig. 1a**. The technique of chemical co-precipitation and *in-situ* growth was considered for the deposition of $Co_3O_4$nanoparticles on rGO nanosheets. The steps are as follows: (i) 0.2 g of dried rGO nanosheets are dispersed in 100 ml of distilled water and sonicated continuously until the rGO sheets are fully dispersed, (ii) 0.458 g of cobalt chloride ($CoCl_2.6H_2O$)are dispersed in 40 ml of water in another beaker and the solution is stirred up to 20 minutes, (iii) it is added to step (ii) cobalt chloride solution with step (i) rGO nanosheets solution slowly, (iv) then 0.2932 g of sodium borohydrate are dispersed in the solution and it can be observed the formation of a black colour precipitate, (v) the precipitate is washed with water and dried at a temperature of 60$^o$C for 12 hours, (vi) the deposition of $Co_3O_4$nanoparticles on rGO nanosheets can be observed. These steps were repeated several times to prepare the required amount of rGO/$Co_3O_4$ nanocomposite nanoparticles.

**2.3. rGO/$Co_3O_4$ characterization**

The TEM (JEOL 2200F, 200KV) results are presented in **Fig. 1b** and the TEM samples were prepared by water diluted rGO/$Co_3O_4$ deposited on the copper grid. Results indicate that the synthesized rGO is a 2-dimensional sheet (left-side image) without any impurities. Based on the *in-situ* growth technique, the cobalt oxide is reduced onto the rGO nanosheets through –COOH groups, and these –COOH groups act as a covalent bond between rGO nanosheets and $Co_3O_4$nanoparticles and they contribute to the stable dilution of hybrid nanomaterial in the de-ionized water. The TEM results of rGO/$Co_3O_4$ clearly show that the $Co_3O_4$ nanoparticles are dispersed on the top surface of the rGO nanosheets.

The Fourier transform infrared (Bruker Equinox V70) spectra of rGO, $Co_3O_{4,}$ and rGO/$Co_3O_4$ are reported in **Fig. 2a**. The IR spectra of rGO nanosheets indicate the presence of various groups, the wavenumber of 1623 cm$^{-1}$ and 1726 cm$^{-1}$ indicates the C=C group and C=O groups. These two groups reveal the availability of –COOH groups on the top layer of rGO nanosheets. Additionally, the wavenumber of 1044 cm$^{-1}$, 1221 cm$^{-1,}$ and 1411 cm$^{-1}$ indicated the formation of C–O–C epoxy or alkoxy groups. The IR spectra of $Co_3O_4$ also presents the various groups, the wavenumbers of 585 cm$^{-1}$ and 672 cm$^{-1}$ are related to the Co–O vibration [62], this shows that the $Co^{2+}$ is oxidized into $Co_3O_4$ nanoparticles. Moreover, the IR spectra of rGO/$Co_3O_4$ nanomaterial exhibit both the peaks of rGO and $Co_3O_4$, which are at wavenumbers of 1623 cm$^{-1}$, 1726 cm$^{-1}$, 1044 cm$^{-1}$, 1221 cm$^{-1}$ and 1411 cm$^{-1}$ related to C=C, C=O, and C–O–C groups for rGO nanosheets and the wavenumbers 585 cm$^{-1}$ and 672 cm$^{-1}$ related to Co–O groups for $Co_3O_4$ nanoparticles.

The XRD (Siemens D-500) patterns of rGO/$Co_3O_4$ and $Co_3O_4$nanoparticlesare reported in **Fig. 2b.** From the XRD patterns, the $Co_3O_4$ nanoparticles planes (111), (220), (311), (400), (511), and (440) and the corresponding 2θ positions 19.03°, 31.31°, 36.87°, 44.81°, 59.42°, and 65.25° match well the JCPDS card No: 073-1701 file, which identifies the cubic structure of the nanoparticles. The rGO nanosheets plane of (002) and the corresponding 2θ position of 24.6° represent the rGO nanosheets peak [53], which can be observed in the rGO/$Co_3O_4$ nanoparticles, and it is indicated in the figure.

The weight composition of rGO nanosheets and $Co_3O_4$ nanoparticles was evaluated by using the magnetic measurement. The composite matrix contains rGO nanosheets and $Co_3O_4$ nanoparticles, in which one offers non-magnetic behaviour (rGO) and the other offers magnetic ($Co_3O_4$) behaviour. The same synthesis procedure is adopted without using rGO nanosheets for the preparation of $Co_3O_4$ nanoparticles for comparison purpose. **Fig. 2c** shows the magnetic (Cryogenics, UK) results of both rGO/$Co_3O_4$hybrid nanoparticles and $Co_3O_4$ nanoparticles. With the use of rGO nanosheets, the final magnetic behavior of rGO/$Co_3O_4$ is decreased, when compared to the magnetic behavior of pure $Co_3O_4$ nanoparticles. The magnetization value of $Co_3O_4$ is 14.23 emu/g [63, 64], with the mixing of rGO nanosheets, its value decreases to 4.67 emu/g. Based on the total magnetization sum rule the decreased magnetization of $Co_3O_4$ is 33%, which means 67% of rGO nanosheets are present in the rGO/$Co_3O_4$ material matrix.

## 3. Evaluation of properties of rGO/$Co_3O_4$ hybrid nanofluids

The rGO/$Co_3O_4$ hybrid nanomaterial is diluted in water to obtain 0.05%, 0.1% and 0.2% particle volume concentrations.

$$\text{Volume concentration, } \phi = \frac{\left[\frac{W_{rGO/Co_3O_4}}{\rho_{rGO/Co_3O_4}}\right]}{\left[\frac{W_{rGO/Co_3O_4}}{\rho_{rGO/Co_3O_4}}\right] + \left[\frac{W_{water}}{\rho_{water}}\right]} \times 100 \quad (1)$$

Where, particle loading (ϕ) (%), density of hybrid nanoparticles ($\rho_{rGO/Co_3O_4}$), weight of hybrid nanoparticles ($W_{rGO/Co_3O_4}$), density of distilled water ($\rho_{water}$), and weight of distilled water($W_{water}$). In Eq. (1), the hybrid nanoparticles density ($\rho_{rGO/Co_3O_4}$) is required and it is evaluated from the law of mixtures equation given by Eq. (2), namely:

$$\text{Density of hybrid nanoparticles, } \rho_{(rGO/Co_3O_4)_p} = \frac{\rho_{rGO} \times W_{rGO} + \rho_{Co_3O_4} \times W_{Co_3O_4}}{W_{rGO} + W_{Co_3O_4}} \quad (2)$$

The values of terms present in Eq. (2) are: density of rGO ($\rho_{rGO}$):1910 kg/m$^3$;, density of $Co_3O_4$,( $\rho_{Co_3O_4}$): 6110 kg/m$^3$, weight of rGO nanosheets ($W_{rGO}$): 0.67 g and weight of $Co_3O_4$ nanoparticles ( $W_{Co_3O_4}$): 0.33 g.

From the magnetic measurement, each 1g of rGO/$Co_3O_4$ hybrid nanoparticles contains 67% of rGO nanosheets (0.67 g) and 33% of $Co_3O_4$ nanoparticles (0.33 g). After substituting these values in Eq. (2), the density of rGO/$Co_3O_4$ hybrid nanomaterial is found to be 3296 kg/m$^3$.

The hybrid nanoparticles thermal conductivity ($k_{rGO/Co_3O_4}$)and specific heat ($C_{p,rGO/Co_3O_4}$) is estimated from the law of mixture equations given by Eq. (3) and (4), namely:

Thermal conductivity of hybrid nanoparticles,

$$k_{(rGO/Co_3O_4)_p} = \frac{k_{rGO} \times W_{rGO} + k_{Co_3O_4} \times W_{Co_3O_4}}{W_{rGO} + W_{Co_3O_4}} \quad (3)$$

Specific heat of hybrid nanoparticles,

$$C_{p,(rGO/Co_3O_4)_p} = \frac{C_{p,rGO} \times W_{rGO} + C_{p,Co_3O_4} \times W_{Co_3O_4}}{W_{rGO} + W_{Co_3O_4}} \quad (4)$$

By substituting in Eq. (3) the values of its variables, $k_{Co_3O_4} = 69 W/mK$, $k_{rGO} = 1000\ W/mK$, $W_{rGO} = 0.67g$ and $W_{Co_3O_4} = 0.33\ g$, the thermal conductivity of rGO/$Co_3O_4$ hybrid nanomaterial calculated is 692.7 $W/mK$.

Similarly, by substituting in Eq. (4) the values of its variables, $C_{p,Co_3O_4} = 460 J/kgK$, $C_{p,rGO} = 710\ J/kgK$, $W_{rGO} = 0.67g$ and $W_{Co_3O_4} = 0.33\ g$,the specific heat of rGO/$Co_3O_4$ hybrid nanomaterial determined is 627.5 J/kg K.

The physical properties of water, rGO, $Co_3O_4$, and rGO/$Co_3O_4$ are presented in **Table 1**. The density of rGO/$Co_3O_4$ hybrid nanomaterial estimated from Eq. (2) is substituted in Eq. (1) to determine the amount of the hybrid nanomaterial required for the preparation of 0.05%, 0.1%, and 0.2% concentrations of 20 liters of hybrid nanofluids and they are 33 g, 66 g, and 132 g, respectively. The synthesized dry powder of rGO/$Co_3O_4$ hybrid nanomaterial and the prepared hybrid nanofluid (0.2 vol. %) are presented in **Fig. 3a** and **3b**.

### 3.1. Thermal conductivity, viscosity, specific heat and density

Each physical property measurement required specific instrumentation, namely: thermal conductivity (KD2 Pro, Decagon Devices Inc., USA), viscosity (A&D viscometer, SV-10, Japan) and specific heat (differential scanning calorimeter-2920 modulated, TA Instruments). The density was measured based on the Archimedes' principle.

The obtained experimental thermal conductivity values of 0% (water), 0.05%, 0.1% and 0.2% concentrations of rGO/$Co_3O_4$ hybrid nanofluids are 0.602, 0.619, 0.625 and 0.648 W/m K, respectively, at a temperature of 20$^o$C and 0.653, 0.709, 0.734 and 0.778 W/m K, respectively, at a temperature of 60$^o$C. When the particle loadings and temperatures increase, the thermal conductivity of nanofluids also increases. For 0.05%, 0.1%, and 0.2% particle loadings, ata temperature of 20$^o$C, the thermal conductivity rise, as compared to water data, is 2.82%, 3.82% and 7.64%, respectively, while at a temperature of 60$^o$C it is 8.58%, 12.40% and 19.14%,, respectively. The thermal conductivity ratio of rGO/$Co_3O_4$ hybrid nanofluids was compared with the data of Taherialekouhi et al. [29] for GO/$Al_2O_3$ nanofluids and Singh et al. [18] for GO/CuO nanofluid; the comparison is presented in **Fig. 4**. The obtained values matched well Taherialekouhi et al. [29] data for GO/$Al_2O_3$

nanofluids and Singh et al. [18] data for GO/CuO nanofluid in the measured volume concentration range. The enhanced thermal conductivity of nanofluids can be explained in terms of Brownian motion and particle migration [65].

The obtained experimental viscosity of rGO/$Co_3O_4$ hybrid nanofluids is qualitatively compared with Kazemi et al. [34] data for graphene-$SiO_2$ nanofluid, the comparison is reported in **Fig. 5**. For the volume concentration of 0.2%, the present rGO/$Co_3O_4$ nanofluids data matches well Kazemi et al. [34] data for graphene-$SiO_2$ nanofluid. By increasing the particle loading, viscosity increases, but it decreases with an increase in temperature. For 0.05%, 0.1% and 0.2% particle loadings, at 20°C the viscosity rise, when compared to water, is 16.66%, 33.33% and 70.83%, respectively, while at 60°C it is 7.59%, 16.45% and 49.36%, respectively. As expected, the presence of the nanoparticles leads to additional resistance between the fluid layers, which results in higher viscosity values for the nanofluids [66].

Considering that there is no specific heat data for graphene based hybrid nanofluids, the obtained experimental specific heat data of rGO/$Co_3O_4$ nanofluids is qualitatively compared with Wole-Osho et al. [22] for $Al_2O_3$-ZnO nanofluids and the comparison is reported in **Fig. 6**. It can be noticed that the nature of the two sets of data is similar, they only differ in magnitude. Wole-Osho et al. [22] used 1:1% of $Al_2O_3$-ZnO for the preparation of nanofluids and the particle specific heat of $Al_2O_3$-ZnO is smaller than that of rGO/$Co_3O_4$. The specific heat of nanofluids decreased with increased particle loading and temperature. For 0.2% particle loading, at temperatures of 20°C and 60°C, the decrease of specific heat, when compared to water data, is 0.04%, and 0.17%, respectively. For fixed heat supply to the base fluid (water) and hybrid nanofluids, the temperature difference is lower for nanofluids than for water. In **Fig. 6** is presented the comparison between the specific heat data of rGO/$Co_3O_4$hybrid nanofluids of the present study and the values obtained with the specific heat correlation proposed by Raud et al. [67], Eq. (5), namely:

$$C_{p,hnf} = \frac{\phi C_{p,hnp}\rho_{hnp} + (1-\phi)C_{p,w}\rho_w}{\phi\rho_{hnp} + (1-\phi)\rho_w} \quad (5)$$

Where, $C_{p,hnf}$ is the hybrid nanofluid, $\phi$ is the particle volume concentration (%), $C_p$ is the specific heat, $\rho$ is the density. The suffixes are hybrid nanofluids (hnf), hybrid nanoparticles (hnp) and water (w).

It can be observed that the experimental specific heat of rGO/$Co_3O_4$ hybrid nanofluids data matches well the theoretical correlation of Raud et al. [67].

There is no experimental data related to density of graphene based hybrid nanofluids; hence the present experimental density of rGO/$Co_3O_4$hybrid nanofluids is compared with the data of Ramalingam et al. [68] for 50:50% W/EG based $Al_2O_3$-SiC hybrid nanofluids, as presented in **Fig. 7**. The trend observed for the hybrid nanofluids density, which decreases with increasing temperature and decreases with increasing particle volume concentration, is similar to that of Ramalingam et al. [68]. The density of rGO/$Co_3O_4$ hybrid nanofluids for 0.2% volume concentration, when compared to the data of Ramalingam et al. [68] for 0.8% volume concentration of 50:50% W/EG based $Al_2O_3$-SiCun-milled and $Al_2O_3$-SiCmilled hybrid nanofluids, presents lower values, which differ by 10.89% and 18.64%, respectively. This apparent discrepancy is due to the use of different hybrid nanofluids and particle volume concentrations. For 0.05%, 0.1%, and 0.2% particle loadings, the density rise at 20$^o$C is 0.11%, 0.22% and 0.45%, respectively, while density rise at 60$^o$C is 0.12%, 0.23% and 0.47%, respectively, when compared to water data. As expected, particle loading increase leads to an increase of the nanofluid density.

The thermal properties of rGO/$Co_3O_4$ nanofluids are required in the evaluation of heat transfer coefficient, friction factor and thermal performance factor. In the present study, the thermophysical properties are measured experimentally and they are compared quantitatively or qualitatively against literature values. Based on this verification, the measured thermophysical properties of hybrid nanofluids are physically sound; therefore, they will be used for the heat transfer calculations.

The Prandtl number of hybrid nanofluids is estimated based on the physical properties and the values are presented in **Fig. 8** for various values of particle loading and temperature. The Prandtl number of 0% (water), 0.05%, 0.1% and 0.2% volume concentration of rGO/$Co_3O_4$ nanofluids, at a temperature of 20$^o$C, is 6.98, 7.3, 7.82 and 9.67, respectively, while at a temperature of 60$^o$C, it is 3.06, 3.29, 3.63, and 4.38, respectively..

**4. Experimental setup**

The experimental forced convection is depicted in **Fig. 9a**; the facility consists of a test tube, flow meter, by-pass valve, constant head pump, chiller, heating element, and U-tube manometer. The test tube is made of copper material with inner diameter ($D_i$) of 0.019 m, outer diameter ($D_o$) of 0.021 m and length ($L$) of 1.750 m. The test tube surface temperature is measured with five J-type thermocouples, which were installed at the location of 0.1875, 0.375, 0.750, 1.125, and 1.312 m from the left side of the tube. The working fluid (water and hybrid nanofluids) inlet ($T_i$) and outlet ($T_o$) temperatures are measured with the other two J-type thermocouples. The uniform heat flux boundary condition of the tube was achieved with nichrome heating element (20 mm gauge, 53.4 $\Omega$/m and 2000 W), which is wrapped circumferentially to the tube. The wrapped test tube was kept in a square duct, which is filled with rock-wool insulation. The square duct is coated with asbestos to avoid further heat loss. The working fluid (water and rGO/$Co_3O_4$-water nanofluids) flow rate in the test facility is maintained with the pump and the fluid flow rate into the test tube is measured with the flow meter. The required flow rate is allowed into the test tube, and the excess fluid, considering that a constant head pump is used, is sent back to the receiver tank through a by-pass valve. The outlet temperature rise of the working fluid (water and rGO/$Co_3O_4$-water) is brought to the atmospheric temperature with a chiller. The drop in pressure across the horizontal tube is measured using the mercury based U-tube manometer.

### 4.1. Longitudinal strip inserts

The aluminum longitudinal strip inserts with three different aspect ratios used in this study are depicted in **Fig. 9b** and the cross-sectional view of the inserts is shown in **Fig. 9c**. The straight strip dimensions and their corresponding hydraulic diameter are listed in **Table 2**. The equivalent hydraulic diameter for the straight strip inserts is calculated using Eq. (6), namely:

$$\text{Hydraulic diameter, } D_h = \frac{4A}{p} \Rightarrow D_h = \frac{4\left[\frac{\pi D_i^2}{4} - W \times H\right]}{[\pi D_i + 2(W + H)]} \qquad (6)$$

The tube inside diameter($D_i$) is 0.019 m, width of the straight strip inserts ($W$)is 0.012, 0.006 and 0.003 m and height of the straight strip inserts ($H$) is 0.012, 0.012 and 0.012 m, then non-dimensional aspect ratio, $AR = W/H,$ which is equal to 1, 2, and 4, respectively. The hydraulic diameter is used to define the mass flow rate $\left(\dot{m} = Re\,\pi D_h \mu/4\right)$ of water or hybrid nanofluids flowing through the test tube with straight strip inserts.

### 4.2. Procedure

For water and hybrid nanofluids circulating in the plain test tube, the fluid flow rates used are: ṁ = 0.035, 0.05, 0.066, 0.083, 0.1, 0.116, 0.133, 0.15, 0.166, 0.183, 0.2, 0.216, 0.233, 0.25 kg/s. Based on the tube diameter($D_i$), absolute viscosity($\mu$) and mass flow rate($\dot{m}$), the Reynolds number is calculated $\left(Re = 4\dot{m}/\pi D_i \mu\right)$ for water and hybrid nanofluids. The Reynolds number for water varies from 2822 to 20158; for 0.05% nanofluid it is varied from 2598 to 18560; for 0.1% nanofluid it is varied from 2372 to 16948 and for 0.2% nanofluid it varies from 1949 to 13921. The difference in Reynolds number values for the hybrid nanofluids, as compared to water at the same mass flow rate, is due to the higher viscosity of the nanofluids. For the case of straight strip inserts, the mass flow rate is adjusted accordingly to meet the corresponding Reynolds number of the fluid.

The benchmark measurements were first conducted with water and then were followed by hybrid nanofluids and with straight inserts. The pump was switched on, and the flow rate of water was fixed at0.035 kg/s; after that, the heating element was switched-on, allowing the system to reach steady-state. When the system achieves steady-state, the thermocouple readings, voltmeter, and ammeter readings were recorded and used later on for the heat transfer analysis. The procedure is repeated for the specified values of flow rate of water and hybrid nanofluids. The pressure difference in the horizontal test tube is used for the friction factor analysis.

### 4.3. Nusselt number evaluation

It is found that the deviation between heat supplied (Eq. 7) and heat absorbed (Eq. 8) is ± 3.4% [59].

The rate of heat supplied, $Q_{input} = V \times I$ (7)

The rate of heat absorbed, $Q_{absorbed} = \dot{m} \times C_p \times (T_{out} - T_{in})$ (8)

Therefore the average of heat supplied, $Q_{input}$ and heat absorbed, $Q_{absorbed}$, $Q_{avg}$ is used in the heat transfer analysis.

Average, $Q_{avg} = \frac{(Q_{input} + Q_{absorbed})}{2}$

From Newton's cooling equation, the of heat transfer coefficient is evaluated using (Eq. 9).

Heat transfer coefficient, $h = \frac{Q_{avg}}{A(T_{wall} - T_{bulk})}$ (9)

Where, $A = \pi D_i L$; $T_{wall} = \frac{T_1 + T_2 + T_3 + T_4 + T_5}{5}$; $T_{bulk} = \frac{T_o + T_i}{2}$

The Nusselt number, $Nu = \frac{h \times D_i}{k}$ (10)

The Prandtl number, $Pr = \frac{\mu \times C_P}{k}$ (11)

### 4.4. Friction factor evaluation

The experimental friction factor of water and $rGO/Co_3O_4$ hybrid nanofluids for the present study was evaluated using Eq. (12) [60], which includes the pressure drop values measured using a U-tube manometer:

The friction factor, $f = \frac{\Delta P}{\left(\frac{L}{D_i}\right)\left(\frac{\rho v^2}{2}\right)}$ (12)

Where, $f$ is the friction factor, $\Delta P$ is the pressure drop (Pa), $L$ is the length of the tube (m), $D_i$ is the diameter of the tube (m), $\rho$ is density of the fluid ($Kg/m^3$) and $v$ is the velocity of the fluid (m/sec).

The dilution of hybrid nanoparticles in the distilled water leads to an increase of the nanofluids density, viscosity and thermal conductivity. These higher values of the properties, in particular density and viscosity, will affect the pressure drop of the fluid.

## 5. Results and discussion

### 5.1. Nusselt number of water and nanofluids in a plain tube

The benchmark validation was conducted for water by comparing the experimental data against the values predicted by the correlations of Dittus and Boelter [69], Gnielinski [70], Notter and Sleicher [71]; this comparison is presented in **Fig. 10**.The correlations of Dittus and Boelter [69], Gnielinski [70], Notter and Sleicher [71] are given by Eq. (13), Eq. (14) and Eq. (15), respectively, as follows:

$$Nu_{DB} = 0.023\, Re^{0.8} Pr^{0.4} \quad (13)$$

$$Nu_G = \frac{\left(\frac{f}{2}\right)(Re - 1000)Pr}{1.07 + 12.7\left(\frac{f}{2}\right)^{0.5}(Pr^{2/3} - 1)} \quad (14)$$

Where, $f = (1.58\, ln(Re) - 3.82)^{-2}$

$0.5 < Pr < 2000$; $2300 < Re < 10^6$

$$Nu_{NS} = 5 + 0.016\, Re^{a} Pr^{b} \quad (15)$$

Where, $a = 0.88 - 0.24/(4 + Pr)$; $b = 0.33 + 0.5e^{-0.6Pr}$

$10^4 < Re < 10^6$;$0 < Pr < 10^4$

It can be observed in **Fig. 10** that the experimental Nusselt number data has a maximum deviation of ±3% against the predictions obtained with Eq. (13) [69], ±1.5% with Eq. (14) [70] and ±2.5% with Eq. (15) [71]. The Nusselt number of rGO/$Co_3O_4$ hybrid nanofluids calculated by using Eq. (10) is reported in **Fig. 11**. The thermal conductivity enhancement for the hybrid nanofluids (Fig. 4) also leads to their Nusselt number enhancement. This enhancement increases with increasing values of particle loading and Reynolds number. The Nusselt number is enhanced by; 3.55% and 13.39% for Re = 2598 and 18560, respectively, at 0.05% concentration; 5.73% and 17.97% for Re = 2372 and 16948, respectively, at 0.1% concentration; and 8.85% and 25.65% for Re = 1949 and 13921, respectively, at 0.2% concentration. The Nusselt number enhancement is due to the increased fluid thermal conductivity, fluid turbulence and particle migration [72,73].

The heat transfer coefficient of rGO/$Co_3O_4$ hybrid nanofluids calculated by using Eq. (10) is reported in **Fig. 12**. The rGO/$Co_3O_4$ nanoparticles dispersed in water lead to an increase of convective heat transfer, which tends to be more pronounced than expected by the increase of thermal conductivity. An eventual explanation may be related to rearrangement of particles and an increase in heat conduction due to shear, which lowers the thickness of the thermal boundary layer. The heat transfer coefficient enhancement increases with increasing values of particle loading and Reynolds number. The heat transfer coefficient is enhanced by: 8.76% and 19.10% for Re = 2598 and 18560, respectively, at 0.05% concentration; 12.42% and 25.43% for Re = 2372 and 16948, respectively, at 0.1% concentration; and 20.52% and 39.12%, for Re = 1949 and 13921, respectively, at 0.2% concentration.

The Nusselt number of rGO/$Co_3O_4$hybrid nanofluids is qualitatively compared with Allahyar et al. [74] data for 97.5% alumina and 2.5% silver hybrid nanomaterial nanofluids, and the comparison is presented in **Fig. 13**. The comparison indicates that for 0.05%, 0.1% and0.2% volume concentration values of rGO/$Co_3O_4$ hybrid nanofluids are obtained higher Nusselt number values by 59.96%, 61.16% and 67.19%, respectively, than those higher values compared to 0.4% volume concentration of Allahyar et al. [74] at Re = 5200; Re = 5200 is the highest Reynolds number for Allahyar et al. [74] data. This difference in Nusselt number establishes that the rGO/$Co_3O_4$ hybrid nanofluids outperform the 97.5% alumina and 2.5% silver hybrid nanofluids.

The Nusselt number of rGO/$Co_3O_4$ hybrid nanomaterial nanofluids is also qualitatively compared with Dalkılıç et al. [75] data for graphite-$SiO_2$/water hybrid nanofluids, and the comparison is presented in **Fig. 14**. The comparison indicates that for the 0.2% concentration of rGO/$Co_3O_4$ hybrid nanofluids, the Nusselt number is higher by 31.73% when compared to that of the 1% volume concentration of Dalkılıç et al. [75] for graphite-$SiO_2$/water hybrid nanofluids at Re = 9500. This difference in Nusselt number indicates that the rGO/$Co_3O_4$/water hybrid nanofluids out perform the graphite graphite-$SiO_2$/water hybrid nanofluids, even when the preparation has a volume concentration five times higher.

**5.2. Nusselt number of water and nanofluids in a plain tube with strip inserts**

The heat transfer influence of water/nanofluids by means of adding straight strip inserts is analyzed. The benchmark analysis was performed for water with the addition of various kinds of straight strip inserts (aspect ratios (AR) of 1, 2, and 4) and Eq. (10) is used again to evaluate the Nusselt number. The obtained data is presented in **Fig. 15**, along with Hsieh and Huang [56] data for AR = 1, 4, and Liu [57] data for AR = 1 for the purpose of comparison. Hsieh and Huang [56] proposed a regression equation for the Nusselt number, when strip inserts are placed into a single-phase fluid flow path, namely:

$$\boldsymbol{Nu = 1.233\ (Gz)^{0.38}\left(\frac{\mu_b}{\mu_w}\right)^{0.14}\left(\frac{D_h}{D_i}\right)^{-0.74}(AR+1)^{0.41}} \quad (16)$$

$$\boldsymbol{1000 < Re < 4000;\ AR = 1, 4}$$

Hsieh and Huang [56] produced experimental data upto Re = 4000, whereas Liu [57] generated experimental data upto Re = 19081. It can be observed in **Fig. 15** the present data for water with strip type inserts (aspect ratios of 1, 2, and 4) matches well Hsieh and Huang [56] data up to Reynolds number of 4000. Liu [57] data for single-phase fluid with straight strip type inserts of aspect ratio of 1 presents higher values of Nusselt number for values of Reynolds number higher than those considered in the present study. The present data clearly shows that by decreasing the aspect ratio of the straight strip inserts from 4 to 1, the Nusselt number increases.

The Nusselt number (Eq. 10) data based on the measurements for water and rGO/$Co_3O_4$ nanofluids with straight strip inserts of AR = 1, 2, and 4 is reported in **Fig. 16**. For water at Reynolds number of 2822 and 20158, the addition of strip insert leads to an increase in Nusselt number, as compared to the plain tube, of; 12.95% and 27.11%, respectively, for AR = 4; 17.09% and 32.34%, respectively, for AR = 2; and 22.54% to 38.72% , respectively, for AR = 1.

The Nusselt number data for the hybrid nanofluid is as follows: with 0.05% concentration of hybrid nanofluid flowing in the test tube at Reynolds number of 2598 and 18560 the addition of strip inserts leads to a Nusselt number increase, as compared to the0.05% concentration in the plain tube, of: 16.12% and 31.72%, respectively, for AR = 4; 21.63% and 36.21%, respectively, for AR = 2; and 28.85% to 46.27%, respectively, for AR = 1. Meanwhile, with 0.1% concentration of hybrid nanofluid flowing in the test tube at Reynolds number of 2372 and 16948 the addition of strip inserts leads to a Nusselt number increase, as compared to the 0.1% concentration in the plain tube, of: 21.29% and 40.48%, respectively, for AR = 4; 25.17% and 48.48%, respectively, for AR = 2; and 31.21% and 57.44%, respectively, for AR = 1. For 0.2% concentration of hybrid nanofluid flowing in the test tube at Reynolds number of 1949 and 13921 the addition of strip inserts leads to a Nusselt number increase, as compared to the 0.2%concentration in the plain tube, of: 26.61% and 50.68%, respectively, for AR = 4; 31.15% and 60.12%, respectively, for AR = 2; and35.49% to 67.62%, respectively, for AR = 1.

For rGO/$Co_3O_4$ hybrid nanofluids with straight strip inserts data is not available in the literature; therefore, the data reported by Sundar et al. [49,50] for MWCNT/$Fe_3O_4$ and ND-Ni hybrid nanofluids with straight strip inserts is used for comparison purposes. They prepared hybrid nanofluids by considering nanotube-spherical shape hybrid nanoparticles and spherical-spherical hybrid nanoparticles. In the present study, nanofluids were prepared 2-dimensional-spherical hybrid nanoparticles. Sundar et al. [59, 60] proposed correlations for hybrid nanofluids with strip type inserts, and the equations are as follows:

The equation of Sundar et al. [59] for MWCNT/$Fe_3O_4$ nanofluids is given below:

$$Nu = 0.0039\, Re^{0.96} Pr^{0.72} (1+\phi)^{0.71} (1+AR)^{0.003} \left(1+\frac{D_h}{D_i}\right)^{-0.08} \quad (17)$$

$$3000 < Re < 22000;\ 0 < \phi < 0.3\%; 4.1 < Pr < 6.4; 0 < AR < 12$$

The equation of Sundar et al. [60] for ND-Ni nanofluids is given below:

$$Nu = 0.02433\, Re^{0.8} Pr^{0.4} (1+\phi)^{1.193} (1+AR)^{0.0291} \left(1+\frac{D_h}{D_i}\right)^{-0.1532} \quad (18)$$

$$3000 < Re < 22000;\ 0 < \phi < 0.3\%; 4.35 < Pr < 5.85;\ 0 < AR < 4$$

The Nusselt number data of rGO/$Co_3O_4$ nanofluids with strip type inserts along with Sundar et al. [59,60] data are reported in **Fig. 17**,and it can be noticed the values, on average, are higher by 22.47% and 35.58% than those for MWCNT/$Fe_3O_4$ [59] and ND-Ni hybrid nanofluids [60], respectively. This improved performance rGO/$Co_3O_4$ hybrid nanofluids may be attributed to the 2-dimensional-spherical shape hybrid nanoparticles.

The rGO/$Co_3O_4$hybrid nanofluids data is regressed with average and standard deviation of 2.86% and 3.69%, respectively; the regression equation is given as follows:

$$Nu = 0.4668\, Re^{0.7941} Pr^{-0.9025} (1+\phi)^{3.280} (1+AR)^{0.04553} \left(1+\frac{D_h}{D_i}\right)^{-0.9609} \quad (19)$$

$$2000 < Re < 21000;\ 5.59 < Pr < 7.85;\ 0 < \phi < 0.2\%;\ 0 < AR < 4$$

The values determined with Eq. (19) are compared against the experimental Nusselt number in **Fig. 18**.

### 5.3. Friction factor of water and nanofluids in a plain tube

The friction factor data for water estimated using Eq. (12) is presented in **Fig. 19**, along with Blasius [76], Eq. 20, and Petukhov [77], Eq. (21), predictions for comparison purposes; the maximum deviation observed is of ±3%.

$$f_B = 0.3164\, Re^{-0.25} \quad (20)$$

$$3000 < \mathrm{Re} < 10^5$$

$$f_P = (0.790\, ln(Re) - 1.64)^{-2} \quad (21)$$

$2300 < \mathrm{Re} < 5 \times 10^6$

The hybrid nanofluids friction factor data is reported in **Fig. 20.** By increasing the particle loading, the friction factor of hybrid nanofluids increases, while an increase in Reynolds number causes it to decrease. For concentrations of 0.05%, 0.1% and 0.2%, the friction factor rise is 1.17% (Re = 2598), 5.2% (Re = 2372) and 8.1% (Re = 1949), respectively, in comparison with water data. Also, for higher values of Reynolds number, and with the concentrations of 0.05%, 0.1% and 0.2%, the friction factor rise is 4.6% (Re = 18560), 8.2% (Re = 16948) and 11.1% (Re = 13921), respectively, in comparison with water data. The friction factor rise of hybrid nanofluids is due to the increased viscosity of the hybrid nanofluids.

The present data for the friction factor of rGO/$Co_3O_4$ hybrid nanomaterial based nanofluids is compared against Madhesh et al. [78] data for Cu-$TiO_2$ hybrid nanomaterial based nanofluids, and the comparison is presented in **Fig. 21**. The friction factor of rGO/$Co_3O_4$ hybrid nanomaterial based nanofluids matches well the friction factor data of Madhesh et al. [78] for the Reynolds number range considered.

### 5.4. Friction factor of water and nanofluids in a plain tube with strip inserts

The penalty in friction factor of water or nanofluids with the addition of straight strip type inserts is analyzed. The benchmark analysis was performed for water with the addition of straight strips with aspect ratios (AR) of 1, 2, and 4.The friction factor is evaluated by using Eq. (12). The obtained values are presented in **Fig. 22** and they are compared against Hsieh and Huang [56] data for AR = 1, 4. Hsieh and Huang [56] generated the following regression equation, which takes into account the insertion of longitudinal strips into a single-phase fluid flow path, namely:

$$\boldsymbol{f = 49.96\, Re^{-0.44}\left(\frac{D_h}{D_i}\right)^{1.18}(AR+1)^{1.53}} \qquad (22)$$

$$\boldsymbol{1000 < Re < 4000;\ AR = 1, 4}$$

The decreased trend of friction factor for water with straight strip inserts (AR = 1, 2 and 4) with increase of Reynolds number was noticed in the present experimental data as well as Hsieh and Huang [56] proposed correlation up to maximum Reynolds number of 4000. The magnitude of friction factor values is different in the present study and Hsieh and Huang [56] data because of various experimental approaches used.

The measurements of the friction factor (Eq. 12) for water and rGO/$Co_3O_4$ nanofluids with the strip inserts with three different aspect ratios (AR = 1, 2, and 4) are presented in **Fig. 23**. In comparison to water flowing through the plain tube, for Reynolds number of 2822 and 20158, the addition of the strip insert leads to the following values of friction factor increase: AR = 4, 15.52% and 18.8%, respectively; AR = 2, 18.85% and 22.09%, respectively; and AR = 1, 21.23% and 27.06%, respectively. Similarly for the 0.05% concentration of hybrid nanofluid flowing through the plain tube, for Reynolds number of 2822 and 20158, the addition of the strip insert leads to the following values of friction factor rise: AR = 4, 20.6% and 26.76%, respectively; AR = 2, 24.32% and 29.49%, respectively; and AR = 1, 228.76% and 30.23%, respectively. For the 0.1% concentration of hybrid nanofluid flowing through the plain tube, for Reynolds number of 2372 and 16948, the addition of the strip insert leads to the following values of friction factor increase: AR = 4, 28.96% and 32.11%, respectively; AR = 2, 34.63% and 37.46%, respectively; and AR = 1, 38.28% and 42.60%, respectively. In addition, for the 0.2% concentration of hybrid nanofluid flowing through the plain tube, for Reynolds number of 1949 and 13921, the addition of the strip insert leads to the following values of friction factor increase: AR = 4, 32.80% to 45.64%, respectively; AR = 2, 38.95% to 46.42%, respectively; and AR = 1, 45.51% to 52.82%, respectively.

The friction factor of rGO/$Co_3O_4$ hybrid nanomaterial nanofluids with strip type inserts data is also not available in the literature. Therefore the Sundar et al. [59, 60] values for MWCNT/$Fe_3O_4$ and ND-Ni hybrid nanomaterial nanofluids with strip inserts are used for comparison purposes. They prepared nanotube-spherical shape and spherical-spherical hybrid nanomaterial based nanofluids, whereas in the present study, 2-dimensional sheet like-spherical shape hybrid nanoparticles based nanofluids were used. The proposed friction factor correlations of Sundar et al. [59, 60] for various hybrid nanomaterial based nanofluids are as follows:

The equation of Sundar et al. [59] for MWCNT/$Fe_3O_4$ nanofluids is given below:

$$f = 0.351\, Re^{-0.2427}(1+\phi)^{0.4039}(1+AR)^{-0.0045}\left(1+\frac{D_h}{D_i}\right)^{-0.22} \quad (23)$$

$3000 < Re < 22000;\ 0 < \phi < 0.3\%;0 < AR < 12$

The equation of Sundar et al. [60] for ND-Ni nanofluids is given below:

$$f = 0.2689\, Re^{-0.2312}(1+\phi)^{0.3556}(1+AR)^{-0.0024}\left(1+\frac{D_h}{D_i}\right)^{-0.083} \quad (24)$$

$3000 < Re < 22000;\ 0 < \phi < 0.3\%;\ 0 < AR < 4$

The friction factor data for rGO/$Co_3O_4$ nanofluids with the addition of straight strip type inserts and its comparison against Sundar et al. [59, 60] data are presented in **Fig. 24**; it can be noticed that on average the values of rGO/$Co_3O_4$ hybrid nanofluids are higher by 20.95% and 21.72% than those of MWCNT/$Fe_3O_4$ and ND-Ni nanofluids. The eventual explanation for this difference may be related to the 2-dimensional sheet like-spherical shape rGO/$Co_3O_4$ hybrid nanoparticles.

The friction factor data of water and rGO/$Co_3O_4$ hybrid nanofluids with the addition of straight strip type inserts data (244 data points) is regressed with an average and standard deviation of 3.024% and 3.714%, respectively; the correlation is given as follows:

$$f = 0.3761\, Re^{-0.2293}(1+\phi)^{0.7204}(1+AR)^{0.06323}\left(1+\frac{D_h}{D_i}\right)^{-0.5892} \quad (25)$$

$2000 < Re < 21000;\ 0 < \phi < 0.2\%;\ 0 < AR < 4$

The values obtained with the correlation Eq. (25) and the experimental friction factor data are presented in **Fig. 25**.

**5.5. Thermal performance factor**

The relation between friction factor rise and Nusselt number enhancement is analyzed by employing the thermal performance factor [79], which is formulated by the following relations:

$$\text{Thermal performance factor, } \eta = \frac{\frac{Nu_{nf}}{Nu_{bf}}}{\left(\frac{f_{nf}}{f_{bf}}\right)^{1/3}} \quad \text{(for nanofluids)} \tag{26}$$

$$\text{Thermal performance factor, } \eta = \frac{\frac{Nu_{insert}}{Nu_{plain}}}{\left(\frac{f_{insert}}{f_{plain}}\right)^{1/3}} \quad \text{(for inserts)} \tag{27}$$

The rGO/$Co_3O_4$ nanofluids led to a significant augmentation of the thermal performance factor (TPF). In comparison with the water data, the Nusselt number increases with the hybrid nanofluids, but the friction factor also increases; however, the effect of the increased friction factor upon the overall performance of the system is minor when compared to the Nusselt number enhancement as demonstrated by the TPF (Eq. 26). The TPF values for the rGO/$Co_3O_4$ nanofluids are reported in **Fig. 26**, and it can be noticed that all TPF of the nanofluids are higher than 1, which indicates that the hybrid nanofluids in turbulent flow lead to performance enhancement. The TPF values of 0.05%, 0.1% and 0.2% nanofluids are 1.09 (Re = 2598), 1.03 (Re = 2372) and 1.06 (Re = 1949), respectively, and for higher Reynolds number values, they are 1.11(Re = 18560), 1.148 (Re = 16948) and 1.213 (Re = 13921), respectively.

Similarly, by means of adding straight strip type inserts in fluid flow, the Nusselt number is enhanced but with a consequent friction factor penalty. To analyze TPF of hybrid nanofluids with and without strip inserts Eq. (27) is used. The TPF values for 0% (water), 0.05%, 0.1%, and 0.2% nanofluids with straight strip inserts for different values of Reynolds number are presented in **Fig. 27**.

The TPF values for straight strip aspect ratio of AR = 4, 2, and 1 are: 1.077, 1.019 and 1.15, respectively, for water with Reynolds number of 2822; 1.201, 1.239, 1.282, respectively, for water with Reynolds number of 20152;1.092, 1.132 and 1.185, respectively, for 0.05% concentration with Reynolds number of 2598; 1.218, 1.251 and 1.341, respectively, for 0.05% concentration with Reynolds number of 18560; 1.115, 1.135 and 1.179, respectively, for 0.1% concentration with Reynolds number of 2372; 1.281, 1.337 and 1.4, respectively, for 0.1% concentration with Reynolds number of 16948; 1.153, 1.177 and 1.197, respectively, for 0.2% concentration with Reynolds number 1949; and 1.331, 1.412 and 1.457, respectively, for 0.2% concentration with Reynolds number of13921.Similar trend of increased overall thermal performance of 28.34% was reported by Ramalingam et al. [68] with the use of $Al_2O_3$:SiC/50:50% water-ethylene glycol hybrid nanofluids for a0.8% particle loading.

The overall thermal performance factor of rGO/$Co_3O_4$ hybrid nanofluids with the addition of strip type inserts exhibit values higher than 1, which, as already mentioned, is an indication that the hybrid nanofluids with the strip inserts in the turbulent regime are beneficial to the system performance.

Potential applications for the combination of rGO/$Co_3O_4$ hybrid nanofluids and longitudinal strip inserts are widespread in what concerns heat exchange equipment. The only requirement is that the nanofluid should operate in a closed loop, while flowing through a tubular system. Shell-and-tube heat exchangers are an example that fits well this requirement. The hybrid nanofluid would flow through the tube side, which will be equipped with the longitudinal strip inserts. Closed loop shell-and-tube heat exchangers are encountered in many industries for process heating/cooling. The effectiveness of a shell-and-tube heat exchanger can have considerable enhancement by the combination of rGO/$Co_3O_4$ hybrid nanofluids and longitudinal strip inserts. Based on industrial experience, just the use of turbulators can lead to an enhancement of up to 20%. This passive heat augmentation technique results in major savings in material, labour, manufacturing and operating costs.

A relevant example is the use of the combination of nanofluids and longitudinal strip inserts in a solar flat plate collector. Sundar et al. [80] report that this combination enhanced the thermal efficiency of the collector by 44.82% with 0.3% volume concentration of $Al_2O_3$/water nanofluid and a longitudinal strip insert of aspect ratio of 1. Preliminary tests indicate that the use of the combination of rGO/$Co_3O_4$ hybrid nanofluids and longitudinal strip inserts leads to further enhancement of the collector thermal efficiency.

## 6. Conclusions

The thermal performance factor was analyzed for rGO/$Co_3O_4$ hybrid nanofluids flowing in a horizontal test tube with straight strip inserts. The thermal conductivity and viscosity were evaluated and for 0.2% concentration at 60$^o$C was observed the highest increase of 19.14% and 70.83%, respectively, when compared to the base fluid (water) data. For concentrations of 0.05%, 0.1% and 0.2% hybrid nanoparticles in water, the Nusselt number increment is 13.39% (Re = 18560), 17.97% (Re = 16948) and 25.60% (Re = 1392), respectively.

For water with addition of straight strip type inserts of AR = 4, 2 and 1, the Nusselt number enhancement is 27.11%, 32.34%, and 38.72%, respectively, whereas, it is further increased to 50.68%, 60.12% and 67.62%, respectively for 0.2% particle concentration hybrid nanofluids for the same strip inserts aspect ratio. Particle concentrations of 0.05%, 0.1%, and 0.2% lead to the following values of in fluid friction penalty: 4.6% (Re = 18560), 8.2% (Re = 16948) and 11.1% (Re = 13921); for Reynolds number of 13921 and 0.2% concentration, the friction factor penalty relative to the insertion of the longitudinal strips of aspect ratio 4, 2 and 1 is 45.64%, 46.42%, and 52.82%, respectively.

The combination of straight strip inserts with the appropriate aspect ratio with rGO/$Co_3O_4$ hybrid nanofluids leads to a significant Nusselt number enhancement. The resulting friction factor penalty, as indicated by the thermal performance factor (TPF) analysis, is negligible when compared to the heat transfer enhancement described by the Nusselt number. The TPF for all the measured cases are above 1, which indicates that the heat transfer benefit is higher than the friction factor penalty. This particular combination has the potential of being used in specific in heat processing applications.

**Nomenclature**

| | | |
|---|---|---|
| $\boldsymbol{A}$ | = | area ($m^2$) |
| $\boldsymbol{D_i}$ | = | inner diameter (m) |
| $\boldsymbol{D_o}$ | = | outer diameter (m) |
| $\boldsymbol{D_h}$ | = | hydraulic diameter (m) |
| $\boldsymbol{f}$ | = | friction factor |
| $\boldsymbol{h}$ | = | heat transfer coefficient ($W/m^2K$) |
| $\boldsymbol{H}$ | = | height (m) |
| $\boldsymbol{k}$ | = | thermal conductivity (W/m K) |
| $\boldsymbol{L}$ | = | length (m) |
| $\boldsymbol{\dot{m}}$ | = | mass flow rate (kg/s) |
| $\boldsymbol{Nu}$ | = | Nusselt number $(\boldsymbol{hD_i/k})$ |
| $\boldsymbol{Re}$ | = | Reynolds number $(\boldsymbol{4\dot{m}/\pi D_i \mu})$ |
| $\boldsymbol{Pr}$ | = | Prandtl number, $(\boldsymbol{\mu \times C_p/k})$ |
| $\boldsymbol{Q}$ | = | heat flow (W) |
| $\boldsymbol{T}$ | = | temperature (°C) |
| $\boldsymbol{W}$ | = | width (m) |

*Symbols*

| | | |
|---|---|---|
| $\boldsymbol{\rho}$ | = | density ($kg/m^3$) |
| $\boldsymbol{\phi}$ | = | particle volume concentration (%) |
| $\boldsymbol{\Delta P}$ | = | pressure drop |
| $\boldsymbol{\mu}$ | = | viscosity (mPa.s) |
| $\boldsymbol{\eta}$ | = | thermal performance factor |

**Appendix:**

The procedure given by Kline and McClintock [81] was used to analyze the uncertainties of the various parameters. The working equations for heat flux, heat transfer coefficient, Nusselt number, Reynolds number and friction factor are presented below. The maximum and minimum range of the instruments used in the present study is listed in **Table 3**, and the uncertainty values are indicated in **Table 4**.

**(i) Heat flux:**

$$q = \frac{Q}{A} \Longrightarrow \frac{V \times I}{\pi D_i L}$$

$$\frac{\delta_q}{q} = \sqrt{\left(\frac{\delta_V}{V} \times 100\right)^2 + \left(\frac{\delta_I}{I} \times 100\right)^2 + \left(\frac{\delta_{D_i}}{D_i} \times 100\right)^2 + \left(\frac{\delta_L}{L} \times 100\right)^2} \quad \text{(A1)}$$

$$\frac{\delta_q}{q} = \sqrt{\left(\frac{1}{220} \times 100\right)^2 + \left(\frac{0.1}{20} \times 100\right)^2 + (0.1)^2 + (0.1)^2} = 0.69\%$$

**(ii) Heat transfer coefficient:**

$$\mathrm{h} = \frac{q}{(T_w - T_b)}$$

$$\frac{\delta_\mathrm{h}}{\mathrm{h}} = \sqrt{\left(\frac{\delta_q}{q} \times 100\right)^2 + \left(\frac{\delta_{T_w}}{T_w} \times 100\right)^2 + \left(\frac{\delta_{T_b}}{T_b} \times 100\right)^2} \quad \text{(A2)}$$

$$\frac{\delta_\mathrm{h}}{\mathrm{h}} = \sqrt{(0.69)^2 + \left(\frac{0.1}{83.78} \times 100\right)^2 + \left(\frac{0.1}{46.32} \times 100\right)^2} = 0.735\%$$

**(iii) Nusselt number:**

$$Nu = \frac{\mathrm{h} D_i}{k}$$

$$\frac{\delta_{Nu}}{Nu} = \sqrt{\left(\frac{\delta_\mathrm{h}}{\mathrm{h}} \times 100\right)^2 + \left(\frac{\delta_{D_i}}{D_i} \times 100\right)^2 + \left(\frac{\delta_k}{k} \times 100\right)^2} \quad \text{(A3)}$$

$$\frac{\delta_{Nu}}{Nu} = \sqrt{(0.735)^2 + (0.1)^2 + (0.1)^2} = 0.7491\%$$

**(iv) Reynolds number:**

$$Re = \frac{4\dot{m}}{\pi D_i \mu}$$

$$\frac{\delta_{Re}}{Re} = \sqrt{\left(\frac{\delta_{\dot{m}}}{\dot{m}} \times 100\right)^2 + \left(\frac{\delta_{D_i}}{D_i} \times 100\right)^2 + \left(\frac{\delta_\mu}{\mu} \times 100\right)^2} \quad \text{(A4)}$$

$$\frac{\delta_{Re}}{Re} = \sqrt{\left(\frac{0.1}{15} \times 100\right)^2 + (0.1)^2 + (0.1)^2} = 0.681\%$$

**(v) Friction factor:**

$$f = \frac{\Delta P}{\left(\frac{L}{D_i}\right)\left(\frac{\rho v^2}{2}\right)}$$

$$\frac{\delta f}{f} = \sqrt{\left(\frac{\delta(\Delta P)}{\Delta P} \times 100\right)^2 + \left(\frac{\delta L}{L} \times 100\right)^2 + \left(\frac{\delta D_i}{D_i} \times 100\right)^2 + \left(\frac{\delta \rho}{\rho} \times 100\right)^2 + \left(\frac{2\,\delta v}{v} \times 100\right)^2} \quad \text{(A5)}$$

$$\frac{\Delta f}{f} = \sqrt{\left(\frac{1}{38.3} \times 100\right)^2 + (0.1)^2 + (0.1)^2 + (0.1)^2 + \left(\frac{2x0.1}{15}\right)^2} = 2.93\%$$

**References:**


[1] S.U.S. Choi, Enhancing thermal conductivity of fluids with nanoparticles. ASME International Mechanical Engineering Congress & Exposition, November 12–17. San Francisco, CA; 1995.

[2] Y. Hwang, J.K. Lee, C.H. Lee, Y.M. Jung, S.I. Cheong, C.G. Lee, B.C. Ku, S.P. Jang, Stability and thermal conductivity characteristics of nanofluids, Thermochimica Acta 455 (2007) 70–74.

[3] O. Mahian, A. Kianifar, S. Wongwises, Dispersion of ZnO nanoparticles in a mixture of ethylene glycol–water, exploration of temperature-dependent density, and sensitivity analysis, J. Cluster Science 24 (2013) 1103–1114.

[4] M. Chandrasekar, S. Suresh, A. Chandra Bose, Experimental investigations and theoretical determination of thermal conductivity and viscosity of $Al_2O_3$/water nanofluid, Exp. Thermal and Fluid Sci. 34 (2010) 210–216.

[5] A. Nasiri, M. Shariaty-Niasar, A. Rashidi, A. Amrollahi, R. Khodafarin, Effect of dispersion method on thermal conductivity and stability of nanofluid, Exp. Thermal and Fluid Sci. 35 (2011) 717–723.

[6] M.J. Assael, I. Metaxa, J. Arvanitidis, D. Christofilos, C. Lioustas, Thermal conductivity enhancement in aqueous suspensions of carbon multi-walled and double-walled nanotubes in the presence of two different dispersants, Int. J. Thermophys. 26 (3) (2005) 647–664.

[7] D. Zhu, X. Li, N. Wang, X. Wang, J. Gao, H. Li, Dispersion behavior and thermal conductivity characteristics of $Al_2O_3$–$H_2O$ nanofluids, Current Appl. Phys. 9(2009) 131–139.

[8] C. Pang, J.-Y. Jung, J.W. Lee, Y.T. Kang, Thermal conductivity measurement of methanol-based nanofluids with $Al_2O_3$ and $SiO_2$ nanoparticles, Int. J. Heat and Mass Transfer 55 (2012) 5597–5602.

[9] M. Hemmat Esfe, S. Saedodin, O. Mahian, S. Wongwises, Thermal conductivity of $Al_2O_3$/water nanofluids, Measurement, correlation, sensitivity analysis, and comparisons with literature reports, J. Thermal Analysis & Calorimetry 117 (2014), 675–681.

[10] S. Pei, H.-M. Cheng, The reduction of graphene oxide, Carbon 50 (2012) 3210–3228.

[11] U. Tanaka, T. Sogabe, H. Sakagoshi, M. Ito, T. Tojo, Anode property of boron-doped graphite materials for rechargeable lithium-ion batteries, Carbon 39 (2001) 931.

[12] F. Ortmann, W.G. Schmidt, F. Bechstedt, Attracted by long-range electron correlation: adenine on graphite, Phys. Review Let. 95 (2005) 186101.

[13] A. Allagui, H. Alnaqbi, A.S. Elwakil, Z. Said, A.A. Hachicha, C. Wang, M.A. Abdelkareem, Fractional-order electric double-layer capacitors with tunable low-frequency impedance phase angle and energy storage capabilities, Applied Physics Letters, 116(1) (2020) 013902.

[14] E. Sadeghinezhad, M. Mehrali, S.T. Latibari, M. Mehrali, S.N. Kazi, C.S. Oon, H.S.C. Metselaar, Experimental investigation of convective heat transfer using graphene nanoplatelet based nanofluids under turbulent flow conditions, Ind. Eng. Chem. Res., 53 (31)(2014) 12455–12465.

[15] M.R. Esfahani, M.R. Nunna, E.M. Languri, K. Nawaz, G. Cunningham, Experimental study on heat transfer and pressure drop of in-house synthesized graphene oxide nanofluids, Heat Transfer Engineering 40 (2019) 1722–1735.

[16] B.R. Ponangi, S. Sumanth, V. Krishna, T.R. Seetharam, K.N.Seetharamu, Heat transfer analysis of radiator using graphene oxide nanofluids, IOP Conf. Series: Materials Science and Engineering 346 (2018) 012032.

[17] F. Soltani, D. Toghraie, A. Karimipour, Experimental measurements of thermal conductivity of engine oil-based hybrid and mono nanofluids with tungsten oxide ($WO_3$) and MWCNTs inclusions, Powder Technology, 371 (2020) 37–44.

[18] J. Singh, R. Kumar, M. Gupta, H. Kumar, Thermal conductivity analysis of GO-CuO/DW hybrid nanofluid, Material Today Proceedings, 28 (3) (2020) 1714-1718.

[19] R.R. Sahoo, V. Kumar, Development of a new correlation to determine the viscosity of ternary hybrid nanofluid, Int. Comm. in Heat and Mass Transfer 111 (2020) 104451.

[20] J.P. Vallejo, E. Sani, G. Żyła, L. Lugo, Tailored silver/graphene nanoplatelet hybrid nanofluids for solar applications, J. Molecular Liquids 296 (2019) 112007.

[21] N. Gupta, S.M. Gupta, S.K. Sharma, Preparation of stable metal/COOH-MWCNT hybrid nanofluid, Material Today Proceedings, 2020 (In press), https://doi.org/10.1016/j.matpr.2020.04.492.

[22] I. Wole-Osho, E.C.Okonkwo, D. Kavaz, S. Abbasoglu, An experimental investigation into the effect of particle mixture ratio on specific heat capacity and dynamic viscosity of $Al_2O_3$-ZnO hybrid nanofluids, Powder Technology 363 (2020) 699-716.

[23] R.R. Sahoo, Thermo-hydraulic characteristics of radiator with various shape nanoparticle-based ternary hybrid nanofluid, Powder Technology 370 (2020) 19-28.

[24] R. Pourrajab, A. Noghrehabadi, E. Hajidavalloo, M. Behbahani, Investigation of thermal conductivity of a new hybrid nanofluids based on mesoporous silica modified with copper nanoparticles: Synthesis, characterization and experimental study, Journal of Molecular Liquids 300 (2020) 112337.

[25] S.K. Singh and J. Sarkar, Improving hydrothermal performance of hybrid nanofluid in double tube heat exchanger using tapered wire coil turbulator, Advanced Powder Technology 31 (5) (2020) 2092-2100.

[26] A. Asadi, I.M. Alarifi, L.K. Foong, An experimental study on characterization, stability and dynamic viscosity of CuO-$TiO_2$/water hybrid nanofluid, Journal of Molecular Liquids 307 (2020) 112987.

[27] M. Sheikholeslami, M. Jafaryar, E. Abohamzeh, A. Shafee, H. Babazadeh, Energy and entropy evaluation and two-phase simulation of nanoparticles within a solar unit with impose of new turbulator, Sustainable Energy Technologies and Assessments 39 (2020) 100727.

[28] M. Sheikholeslami, M. Jafaryar, A. Shafee, H. Babazadeh, Acceleration of discharge process of clean energy storage unit with insertion of porous foam considering nanoparticle enhanced paraffin, Journal of Cleaner Production 261 (2020) 121206.

[29] R. Taherialekouhi, S. Rasouli, A. Khosravi, An experimental study on stability and thermal conductivity of water-graphene oxide/aluminum oxide nanoparticles as a cooling hybrid nanofluid, Int. J. Heat and Mass Transfer 145 (2019) 118751.

[30] M. Afrand, Experimental study on thermal conductivity of ethylene glycol containing hybrid nano-additives and development of a new correlation, Applied Thermal Engineering 110 (2017) 1111–1119.

[31] Z. Said, M.A. Abdelikareem, H. Rezk, A.M. Nassef, H.Z. Atwany, Stability, thermophysical and electrical properties of synthesized carbon nanofiber and reduced-graphene oxide-based nanofluids and their hybrid along with fuzzy modeling approach, Powder Technology 364 (2020) 795–809.

[32] M. Gupta, V. Singh, Z. Said, Heat transfer analysis using zinc ferrite/water (Hybrid) nanofluids in a circular tube: An experimental investigation and development of new

correlations for thermophysical and heat transfer properties, Sustainable Energy Technologies and Assessments 39 (2020) 100720.

[33] M.J. Nine, M. Batmunkh, J.H. Kim, H.S. Chung, H.M. Jeong, Investigation of $Al_2O_3$-MWCNTs hybrid dispersion in water and their thermal characterization, J. Nanosci. Nanotechnol. 12 (2012) 4553–4559.

[34] I. Kazemi, M. Sefid, M. Afrand, A novel comparative experimental study on rheological behavior of mono & hybrid nanofluids concerned graphene and silica nano-powders: Characterization, stability and viscosity measurements, Powder Technology 366 (2020) 216–229.

[35] O. Soltani, M. Akbari, Effects of temperature and particles concentration on the dynamic viscosity of MgO-MWCNT/ethylene glycol hybrid nanofluid: experimental study, Physica E: Low-dimensional Systems and Nanostructures 84 (2016) 564–570.

[36] A. Rahimi, M. Rahjoo, S.S. Hashemi, M.R. Sarlak, M.H. Malekshah, E.H. Malekshah, Combination of Dual-MRT lattice Boltzmann method with experimental observations during free convection in enclosure filled with MWCNT-MgO/Water hybrid nanofluid, Thermal Science and Engineering Progress 5 (2018) 422-436.

[37] M.A. Mansour, S. Siddiq, R.S.R. Gorla, A.M. Rashad, Effects of heat source and sink on entropy generation and MHD natural convection of $Al_2O_3$-Cu/water hybrid nanofluid filled with square porous cavity, Thermal Science and Engineering Progress 6 (2018) 57-71.

[38] T. Tayebi, H.F. Öztop, A.J. Chamkha, Natural convection and entropy production in hybrid nanofluid filled-annular elliptical cavity with internal heat generation or absorption, Thermal Science and Engineering Progress 19 (2020) 100605.

[39] M.Z. Saghir and A.M. Bayomy, Heat enhancement and heat storage for a ternary mixture in a circular pipe, Thermal Science and Engineering Progress 5 (2018) 32-43.

[40] Y. Shin, J. Ham, T. Boldoo, H. Cho, Magnetic effect on the enhancement of photo-thermal energy conversion efficiency of MWCNT/$Fe_3O_4$ hybrid nanofluid, Solar Energy Materials and Solar Cells 215 (2020) 110635.

[41] S.Goudarzi, M. Shekaramiz, A. Omidvar, E. Golab, A. Karimipour, A. Karimipour, Nanoparticles migration due to thermophoresis and Brownian motion and its impact on Ag-MgO/Water hybrid nanofluid natural convection, Powder Technology 375 (2020) 493-503.

[42] W.T. Urmi, M.M. Rahman, W.A.W. Hamzah, An experimental investigation on the thermophysical properties of 40% ethylene glycol based $TiO_2$-$Al_2O_3$ hybrid nanofluids, International Communications in Heat and Mass Transfer 116 (2020) 104663.

[43] A.Boroomandpour, D. Toghraie, M. Hashemian, A comprehensive experimental investigation of thermal conductivity of a ternary hybrid nanofluid containing MWCNTs- titania-zinc oxide/water-ethylene glycol (80:20) as well as binary and mono nanofluids, Synthetic Metals 268 (2020) 116501.

[44] H.T. Kadhim, F. A. Jabbar, A. Rona, Cu-$Al_2O_3$ hybrid nanofluid natural convection in an inclined enclosure with wavy walls partially layered by porous medium, International Journal of Mechanical Sciences 186 (2020) 105889.

[45] L.R. Oliveira, S.R.F.L. Ribeiro, M.H.M. Reis, V.L. Cardoso, E.P.B. Filho, Experimental study on the thermal conductivity and viscosity of ethylene glycol-based nanofluid containing diamond-silver hybrid material, Diamond & Related Materials 96 (2019) 216–230.

[46] S.H. Qing, W. Rashmi, M. Khalid, T.C.S.M. Gupta, M. Nabipoor, M.T. Hajibeigy, Thermal conductivity and electrical properties of hybrid $SiO_2$-graphene naphthenic mineral oil nanofluid as potential transformer oil, Materials Research Express 4 (2017) 015504.

[47] S.S. Jyothirmayee Aravind, S. Ramaprabhu, Graphene wrapped multiwalled carbon nanotubes dispersed nanofluids for heat transfer applications, J. Applied Physics 112 (2012) 124304 1–9.

[48] T.T. Baby, S. Ramaprabhu, Synthesis and nanofluid application of silver nanoparticles decorated graphene, J. Mater. Chem., 21 (2011) 9702–9709.

[49] Q. Su, W. Yuan, L. Yao, Y. Wu, J. Zhang, G. Du, Microwave-assisted synthesis of $Co_3O_4$–graphene sheet-on-sheet nanocomposites and electrochemical performances for lithium ion batteries, Materials Research Bulletin 72 (2015) 43–49.

[50] C. Peng, B. Chen, Y. Qin, S. Yang, C. Li, Y. Zuo, S. Liu, J. Yang, Facile ultrasonic synthesis of CoO quantum dot/graphene nanosheet composites with high lithium storage capacity, ACS Nano 6(2)(2012) 1074–1081.

[51] Y. Liang, Y. Li, H. Wang, J. Zhou, J. Wang, T. Regier, H. Dai, $Co_3O_4$ nanocrystals on graphene as a synergistic catalyst for oxygen reduction reaction, Nature Materials 10 (2011) 780–786.

[52] P. Shi, X. Dai, H. Zheng, D. Li, W. Yao, C. Hu, Synergistic catalysis of $Co_3O_4$ and graphene oxide on $Co_3O_4$/GO catalysts for degradation of Orange II in water by advanced oxidation technology based on sulfate radicals, Chemical Engineering Journal 240 (2014) 264–270.

[53] C. Xiang, M. Li, M. Zhi, A. Manivannan, N. Wu, A reduced graphene oxide/$Co_3O_4$ composite for supercapacitor electrode, J. Power Sources 226 (2013) 65–70.

[54] L. Syam Sundar, M.K. Singh, M.C. Ferro, Antonio C.M. Sousa, Experimental investigation of the thermal transport properties of graphene oxide/$Co_3O_4$ hybrid nanofluids, Int. Communications in Heat and Mass Transfer 84 (2017) 1–10.

[55] S.-S. Heish, M.-Y. Wen, Developing three dimensional laminar mixed convection in a circular tube inserted with longitudinal strip inserts, Int. J. Heat Mass Transfer 19 (1996) 299–310.

[56] S.-S. Hsieh, I.-W. Huang, Heat transfer and pressure drop of laminar flow in horizontal tubes with/without longitudinal strip inserts, J. Heat Transfer 122(2000) 465–475.

[57] M.-H. Liu, Turbulent Heat Transfer in Horizontal Circular Tube with Strip Inserts, M.S. thesis, Department of Mechanical Engineering, National Sun Yat-Sen University, Chinese, 1996.

[58] L. Syam Sundar, K.V. Sharma, Heat transfer enhancements of low volume concentration $Al_2O_3$ nanofluid and with longitudinal strip inserts in a circular tube, Int. J. Heat and Mass Transfer 53 (2010) 4280–4286.

[59] L. Syam Sundar, G. Otero-Irurueta, M.K. Singh, A.C.M. Sousa, Heat transfer and friction factor of multi-walled carbon nanotubes–$Fe_3O_4$ nanocomposite nanofluids flow in a tube with/withoutlongitudinal strip inserts, Int. J. Heat and Mass Transfer 100 (2016) 691–703.

[60] L. Syam Sundar, M.K. Singh, A.C.M. Sousa, Heat transfer and friction factor of nanodiamond-nickel hybrid nanofluids flow in a tube with longitudinal strip inserts, Int. J. Heat and Mass Transfer 121 (2018) 390–401.

[61] W.S. Hummers, R.E. Offeman, Preparation of Graphitic Oxide. J. American Chemical Society 80 (1958) 1339.

[62] F. Mohandes, F. Davar, M. Salavati-Niasari, Preparation of $Co_3O_4$ nanoparticles by nonhydrolytic thermolysis of $[Co(Pht)(H_2O)]_n$ polymers, J. Magnetism and Magnetic Materials 322 (2010) 872–877.

[63] P. Dutta, M.S Seehra, S. Thota, J. Kumar, A comparative study of the magnetic properties of bulk and nanocrystalline Co3$O_4$, J. Phys.: Condens. Matter 20 (2008) 015218 1-8.

[64] H.T. Yang, Y.K. Su, C.M. Shen, T.Z. Yang, H.J. Gao, Synthesis and magnetic properties of $\varepsilon$-cobalt nanoparticles, Surf. Interface Anal. 36 (2004) 155–160.

[65] P.S. Kishore, V. Shireesha, V. Sree Harsha, V. Dharma Rao, A. Brusly Solomon, Preparation, characterization and thermo-physical properties of Cu-graphene nanoplatelets hybrid nanofluids. Materials Today: Proceedings 27(1) (2020) 610-614.

[66] A. Zareie, M. M. Akbari, Hybrid nanoparticles effects on rheological behavior of water-EG coolant under different temperatures: an experimental study, J. Molecular Liquids 230 (2017) 408–414.

[67] R. Raud, B. Hosterman, A. Diana, T.A. Steinberg, G. Will, Experimental study of the interactivity, specific heat, and latent heat of fusion of water based nanofluids, Applied Thermal Engineering 117 (2017) 164–168.

[68] S. Ramalingam, R. Dhairiyasamy, M. Govindasamy, Assessment of heat transfer characteristics and system physiognomies using hybrid nanofluids in an automotive radiator, Chemical Engineering & Processing: Process Intensification 150 (2020) 107886.

[69] F.W. Dittus, L.M.K. Boelter, Heat Transfer in Automobile Radiators of theTubular Type, vol. 11, University California Publication in Engineering, 1930.

[70] V. Gnielinski, New equations for heat and mass transfer in turbulent pipe and channel flow, Int. Chemical Engineering 16 (1976) 359–368.

[71] R.H. Notter, C.A. Sleicher, A solution to the turbulent Graetz problem–III Fully developed and entry region heat transfer rates, Chemical Engineering Science 27 (1972) 2073–2093.

[72] S. Suresh, K.P. Venkitaraj, P. Selvakumar, M. Chandrasekar, Effect of $Al_2O_3$-Cu/water hybrid nanofluid in heat transfer, Exp. Thermal and Fluid Sci. 38 (2012) 54–60.

[73] L. Syam Sundar, M.K. Singh, A.C.M. Sousa, Enhanced heat transfer and friction factor of MWCNT-$Fe_3O_4$/water hybrid nanofluids, Int. Comm. in Heat and Mass Transfer 52 (2014) 73–83.

[74] H.R. Allahyar, F. Hormozi, B. ZareNezhad, Experimental investigation on the thermal performance of a coiled heat exchanger using a new hybrid nanofluid,Exp. Therm. Fluid Sci. 76 (2016) 324–329.

[75] A.S. Dalkılıça, O. Alperen Türk, H. Mercan, S. Nakkaew, S. Wongwises, An experimental investigation on heat transfer characteristics of graphite-$SiO_2$/water hybrid nanofluid flow in horizontal tube with various quadchanneltwisted tape inserts, International Communications in Heat and Mass Transfer 107 (2019) 1–13.

[76] H. Blasius, The boundary layers in fluids with little friction, Z. Math. Phys. 56 (1908) 1–37.

[77] B.S. Petukhov, Heat transfer and friction in turbulent pipe flow with variable physical properties. JP. Hartnett and TF. Irvine, (Eds.), Advances in Heat Transfer, Academic Press, NY, (1970) 504–564.

[78] D. Madhesh, R. Parameshwaran, S. Kalaiselvam, Experimental investigation on convective heat transfer and rheological characteristics of Cu-$TiO_2$ hybrid nanofluids, Exp. Thermal and Fluid Sci. 52 (2014) 104–115.

[79] A.E. Bergles, A.R. Blumenkrantz, J. Taborek, Performance evaluation criteria for enhanced heat transfer surfaces, Journal of Heat Transfer 2 (1974) 239–243.

[80] L. Syam Sundar, A. Kirubeil, V. Punnaiah, M.K. Singh, A.C.M. Sousa, Effectiveness analysis of solar flat plate collector with $Al_2O_3$ water nanofluids and with longitudinal strip inserts, Int. J. Heat and Mass Transfer 127 (2018) 422–435.

[81] S.J. Kline, F.A. McClintock, Describing uncertainties in single sample experiments, Mech. Eng., 75(1) (1953) 3–8.

**Table 1:** The physical properties of water, rGO, $Co_3O_4$ and rGO/$Co_3O_4$ nanoparticles at 20°C

| Substance | $\rho$, (kg/m³) | $k$, (W/m K) | $C_p$, (J/Kg K) | $\mu$, (mPa.s) |
|---|---|---|---|---|
| Water | 998.5 | 0.602 | 4178 | 0.89 |
| rGO | 1910 | 1000 | 710 | ---- |
| $Co_3O_4$ | 6110 | 69 | 460 | ---- |
| rGO/$Co_3O_4$ | 3296 | 692.7 | 627.5 | ---- |

**Table: 2** Dimensions of the longitudinal strip inserts

| Aspect ratio, $(AR = W/H)$ | Width $(W)$, (m) | Height $(H)$, (m) | Hydraulic diameter, $D_h$ (m) | $\frac{D_h}{D_i}$ |
|---|---|---|---|---|
| AR = 1 | 0.012 | 0.012 | 0.005183 | 0.2727 |
| AR = 2 | 0.012 | 0.006 | 0.008839 | 0.4652 |
| AR = 4 | 0.012 | 0.003 | 0.011032 | 0.5806 |

**Table 3** Uncertainties of instruments

| Instrument | Variable measured | Range | Least division | Minimum value of the experiment | Maximum value of the experiment | Uncertainty (%) |
|---|---|---|---|---|---|---|
| Thermocouples | Fluid inlet and out temperature | 0-120°C | 0.1°C | 31.25°C | 46.32°C | 0.2158 |
| Thermocouples | Wall temperature | 0-120°C | 0.1°C | 45.66°C | 83.78°C | 0.1193 |
| U-tube manometer | Height of the $CCl_4$ | 0-50 cm | 1 mm | 2.0 cm | 38.3 cm | 0.02610 |
| Totalizer | Cold fluid mass flow rate | 0–99999 L | 0.1 L | 1 L | 15 L | 0.666 |
| Properties | Thermal conductivity, density, specific heat, viscosity | | | | | 0.1 |
| Dimensions | Diameter, area | | | | | 0.1 |

**Table 4** Uncertainty values

| Parameter | Uncertainty, (%) |
|---|---|
| Heat flux | 0.69 |
| Heat transfer coefficient (h) | 0.735 |

| | |
|---|---|
| Nusselt number (Nu) | 0.7491 |
| Reynolds number (Re) | 0.681 |
| Friction factor (f) | 2.93 |

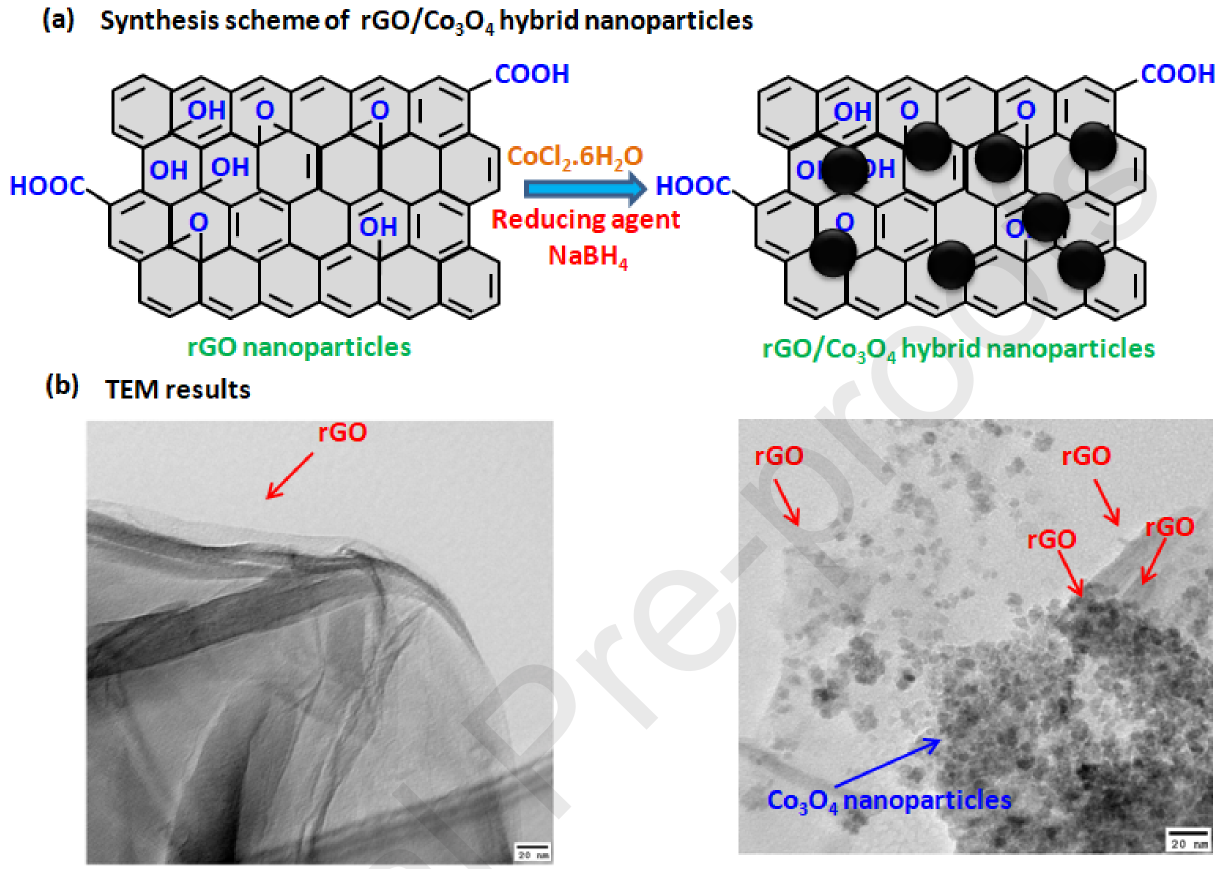


**Fig. 1**(a) Synthesis process and (b) TEM results

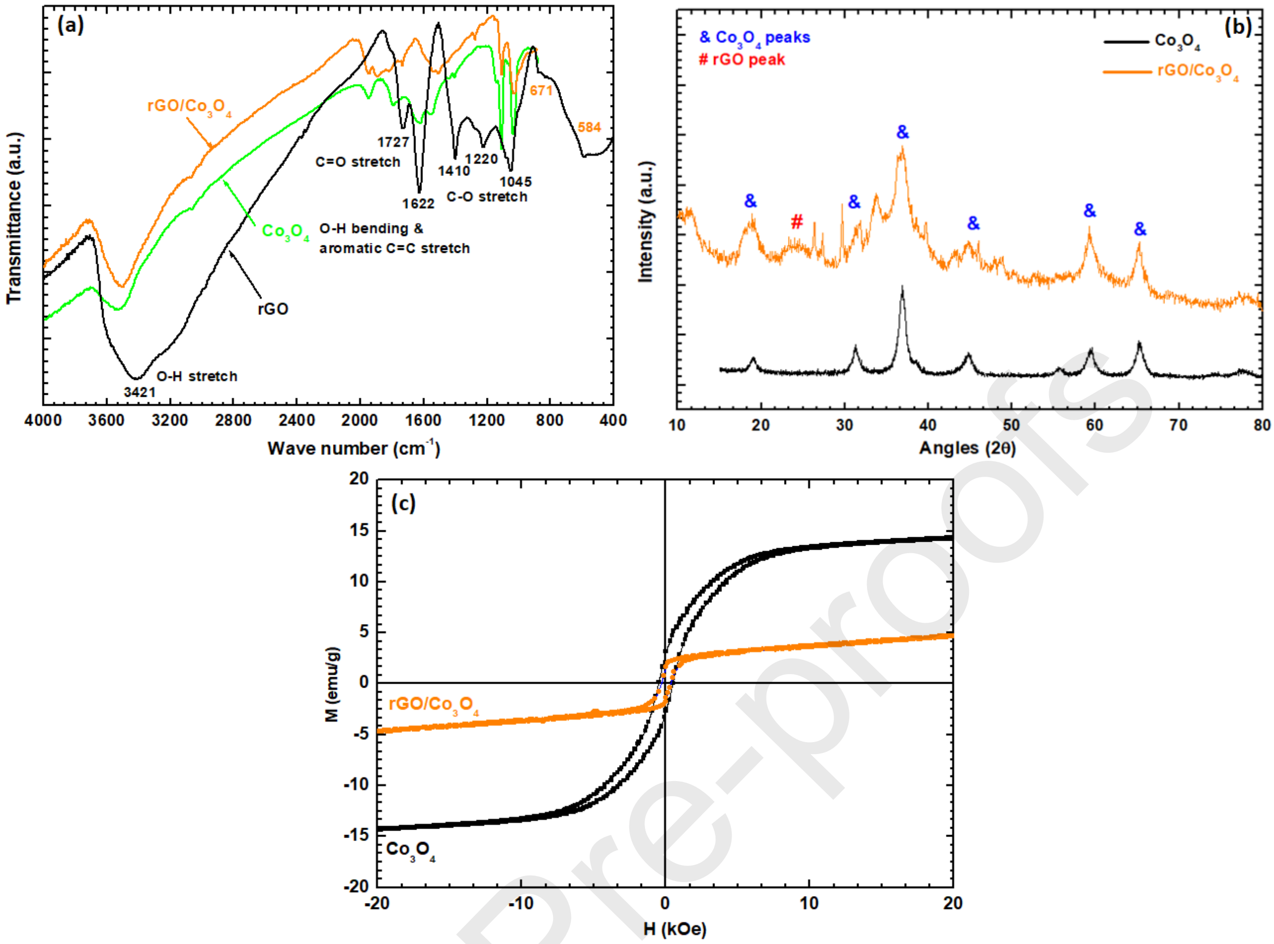


**Fig. 2** (a) FTIR results, (b) XRD patterns and (c) magnetic measurement results

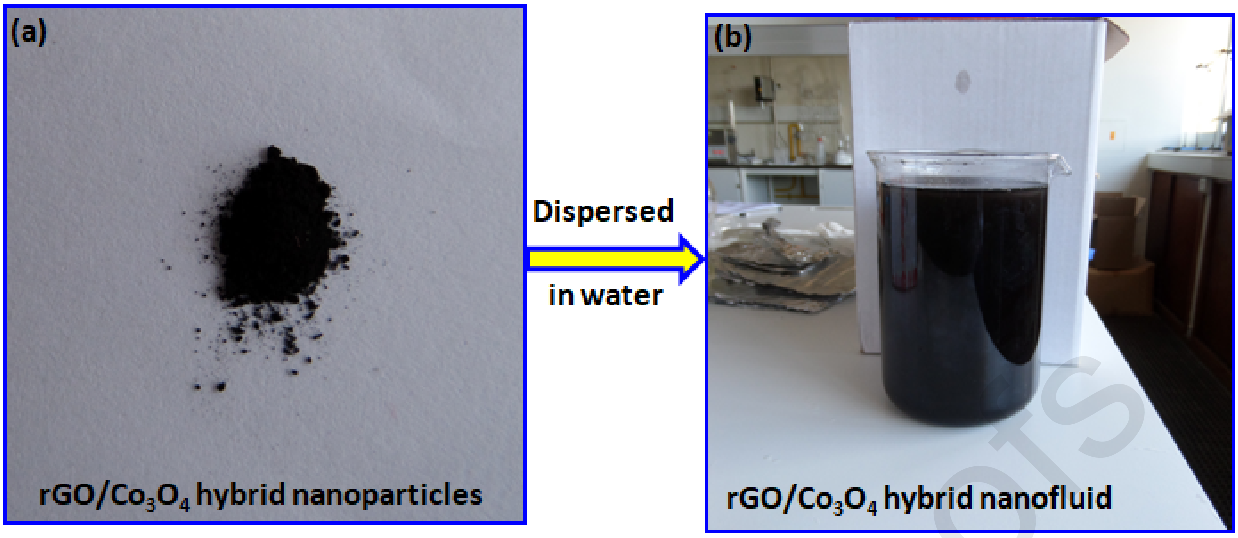


**Fig. 3** (a) Dry powder of rGO/$Co_3O_4$ nanoparticles and (b) Final 0.2% nanofluid sample

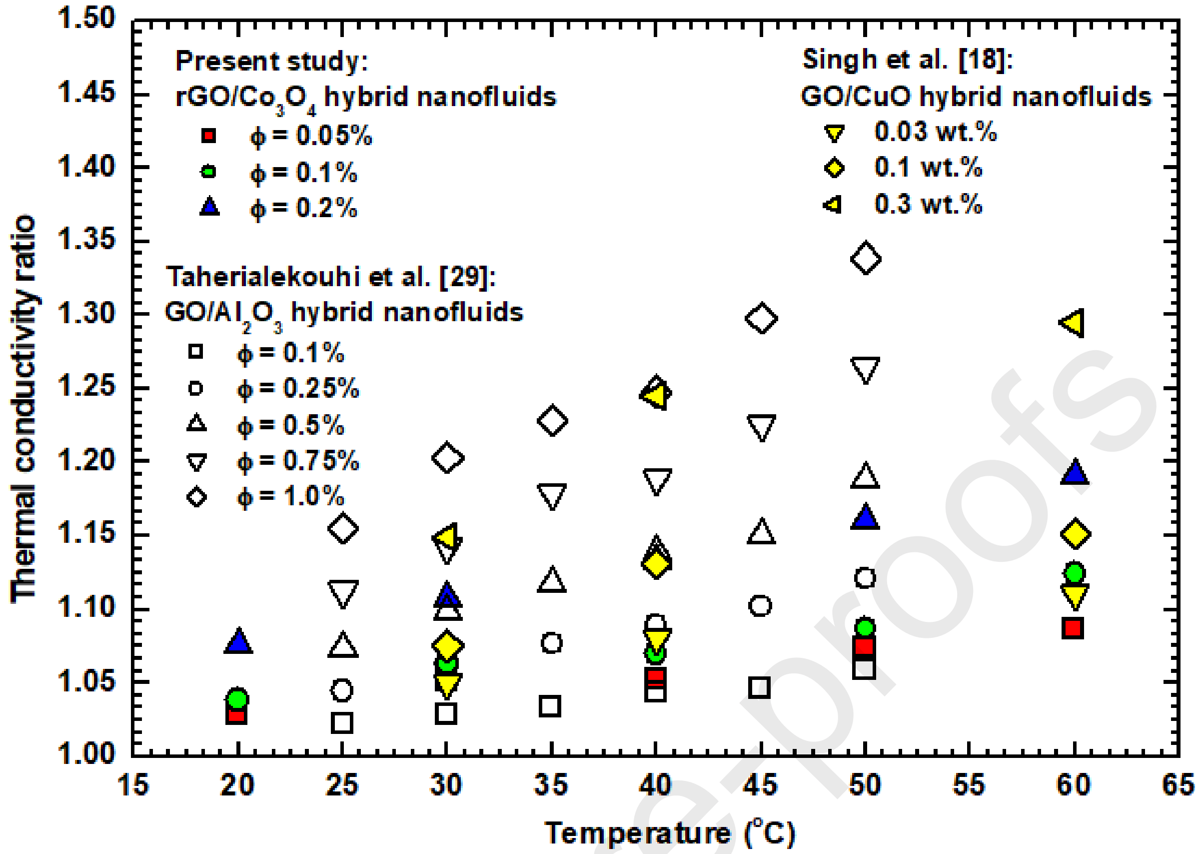


**Fig. 4**Comparison ofrGO/$Co_3O_4$ nanofluidsthermal conductivity ratioagainst the data of Taherialekouhi et al. [29] for GO/$Al_2O_3$ nanofluid and Singh et al. [18] for GO/CuO nanofluid

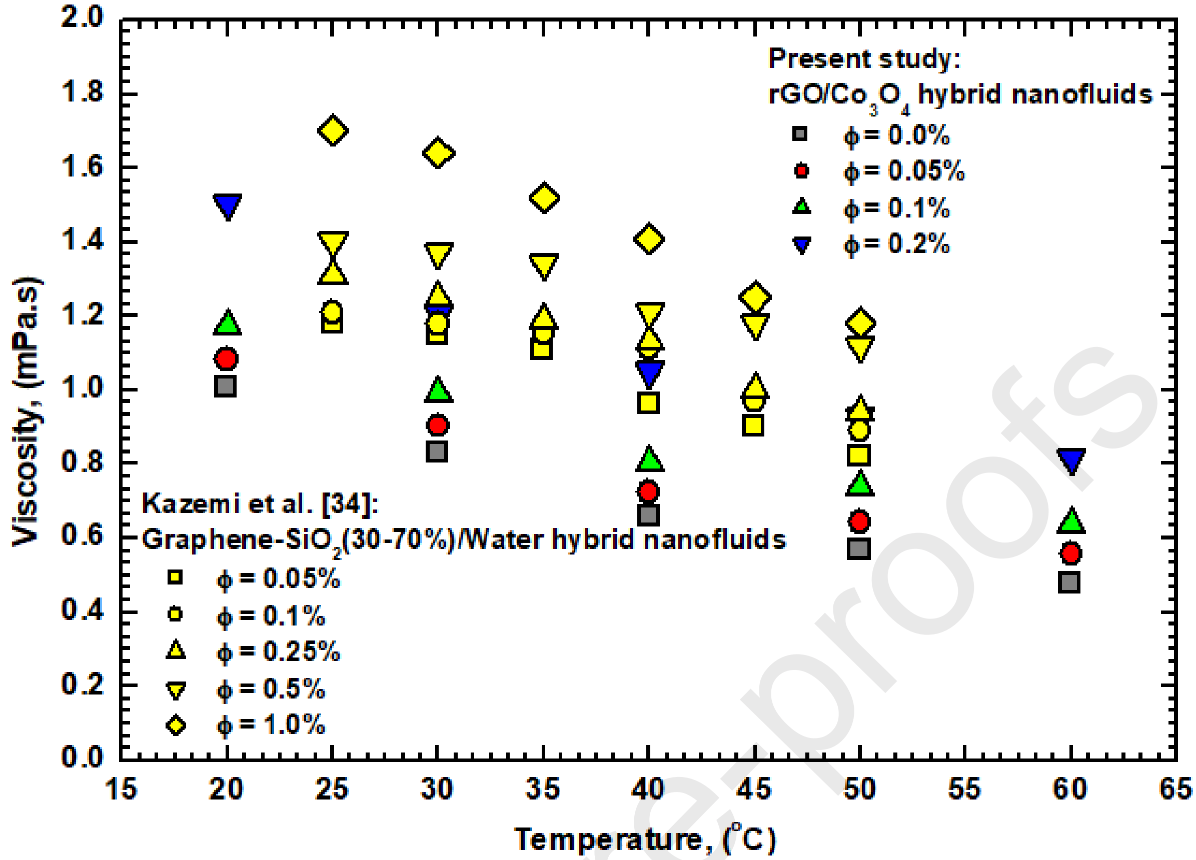


**Fig. 5**Comparison of rGO/$Co_3O_4$ nanofluid viscosity against the data of Kazemi et al. [34] for Graphene-$SiO_2$ nanofluid

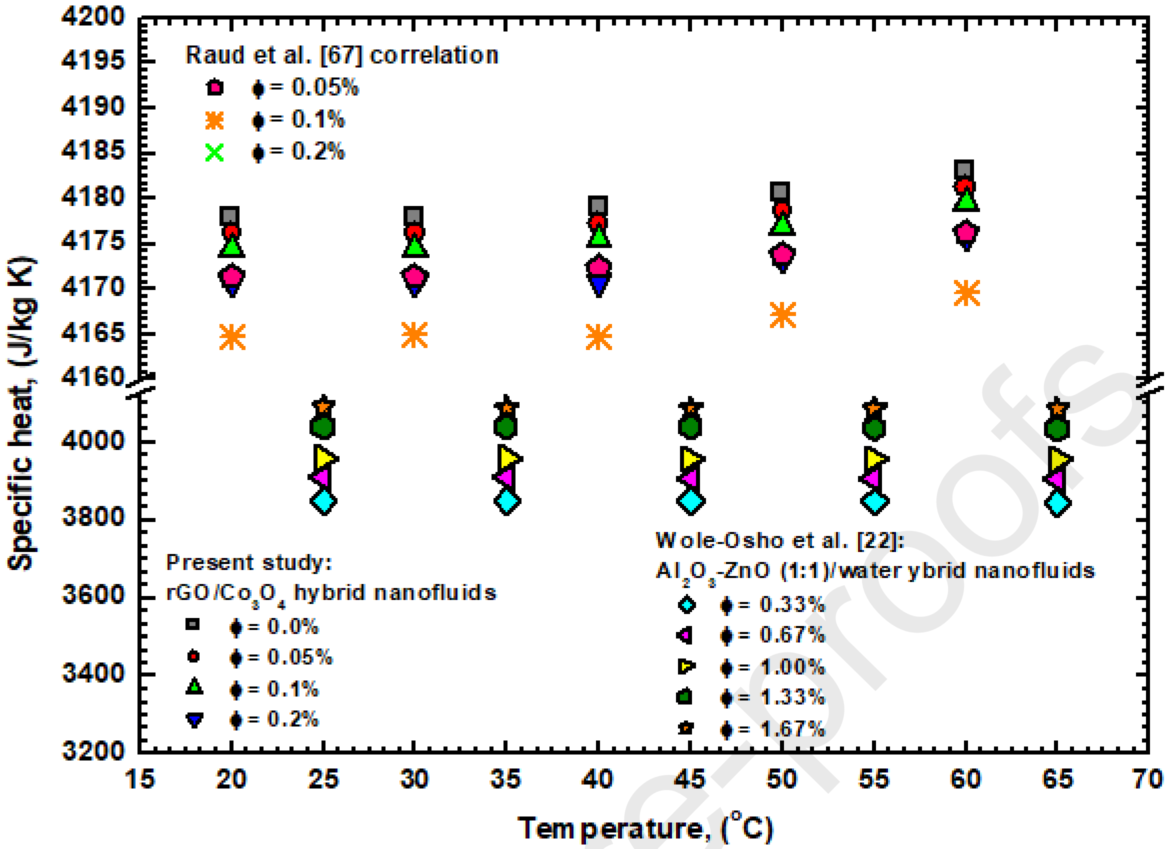


**Fig. 6** Comparison of rGO/$Co_3O_4$ nanofluids specific heat against the data of Wole-Osho et al. [22] for $Al_2O_3$-ZnO nanofluids and the predictions of Raud et al. [67] correlation.

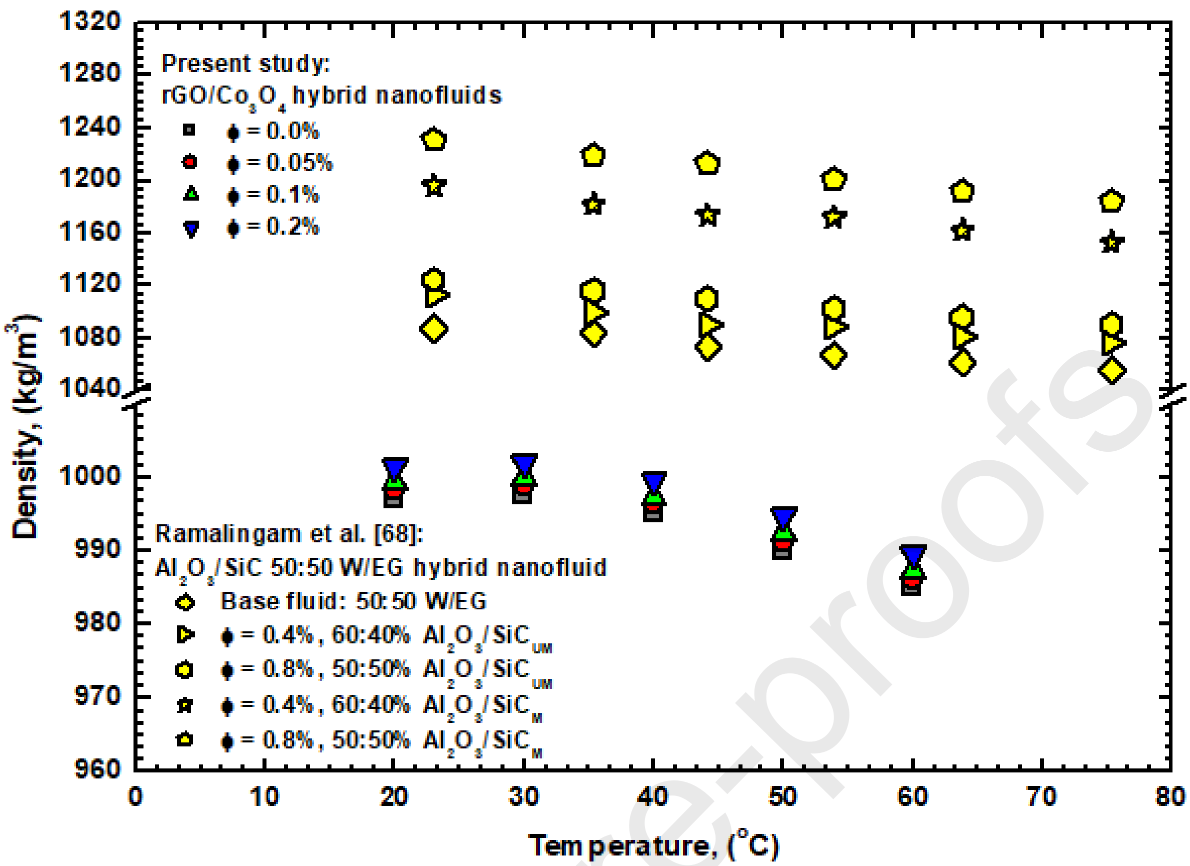


**Fig. 7** Comparison of rGO/$Co_3O_4$ nanofluidsdensityagainst the data of Ramalingam et al. [68] for $Al_2O_3$/SiC 50:50 W/EG hybrid nanofluids.

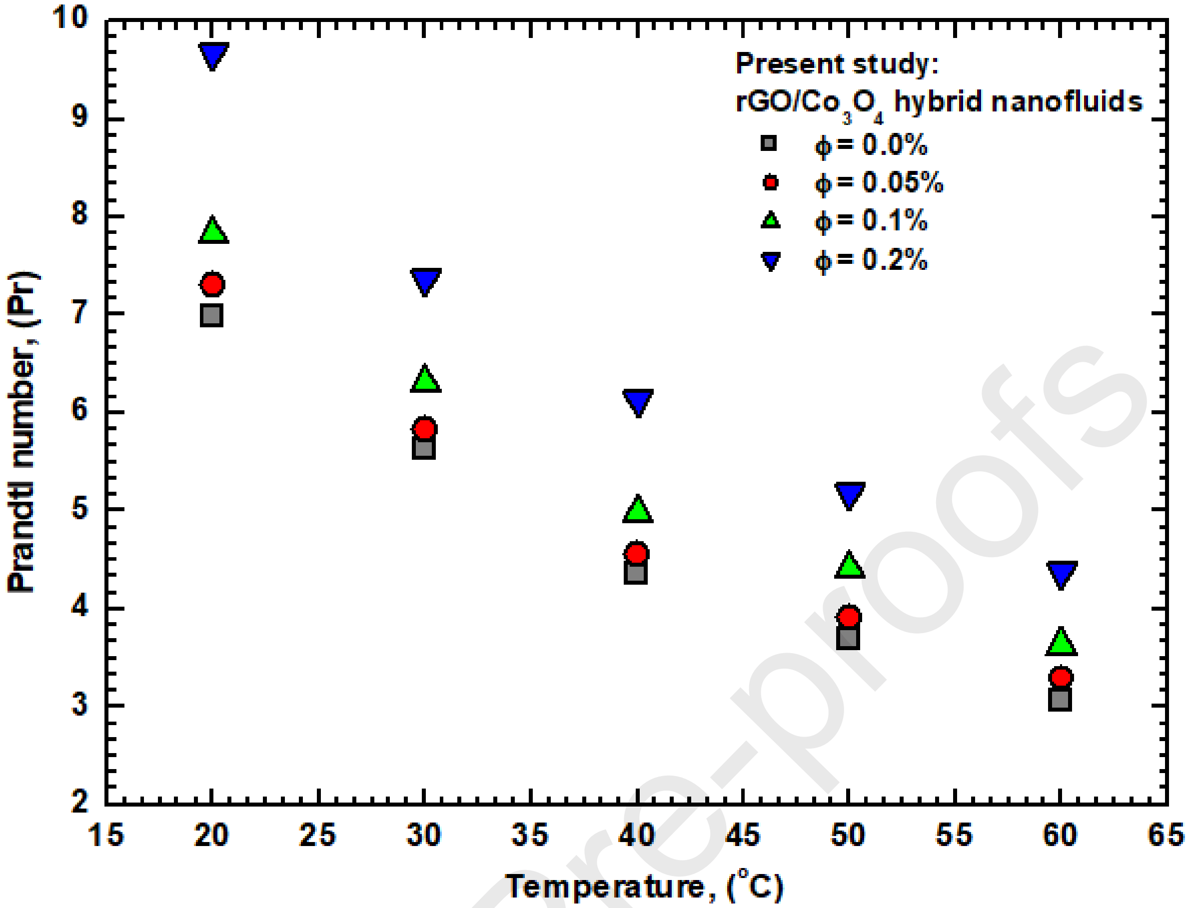


**Fig. 8** Prandtl number of rGO/$Co_3O_4$ hybrid nanofluids fordifferent values of particle loading and concentration

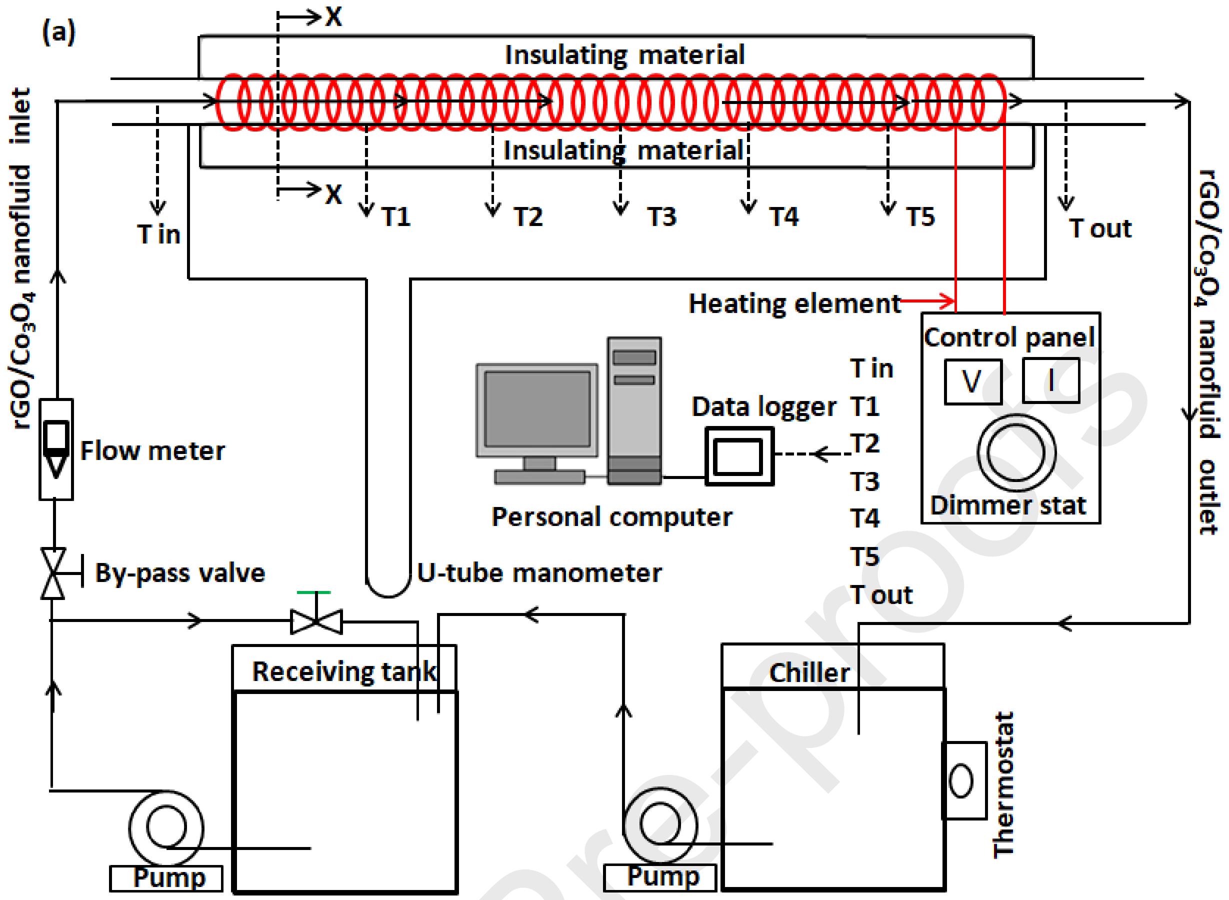


**Fig. 9(a)** Experimental test facility schematic

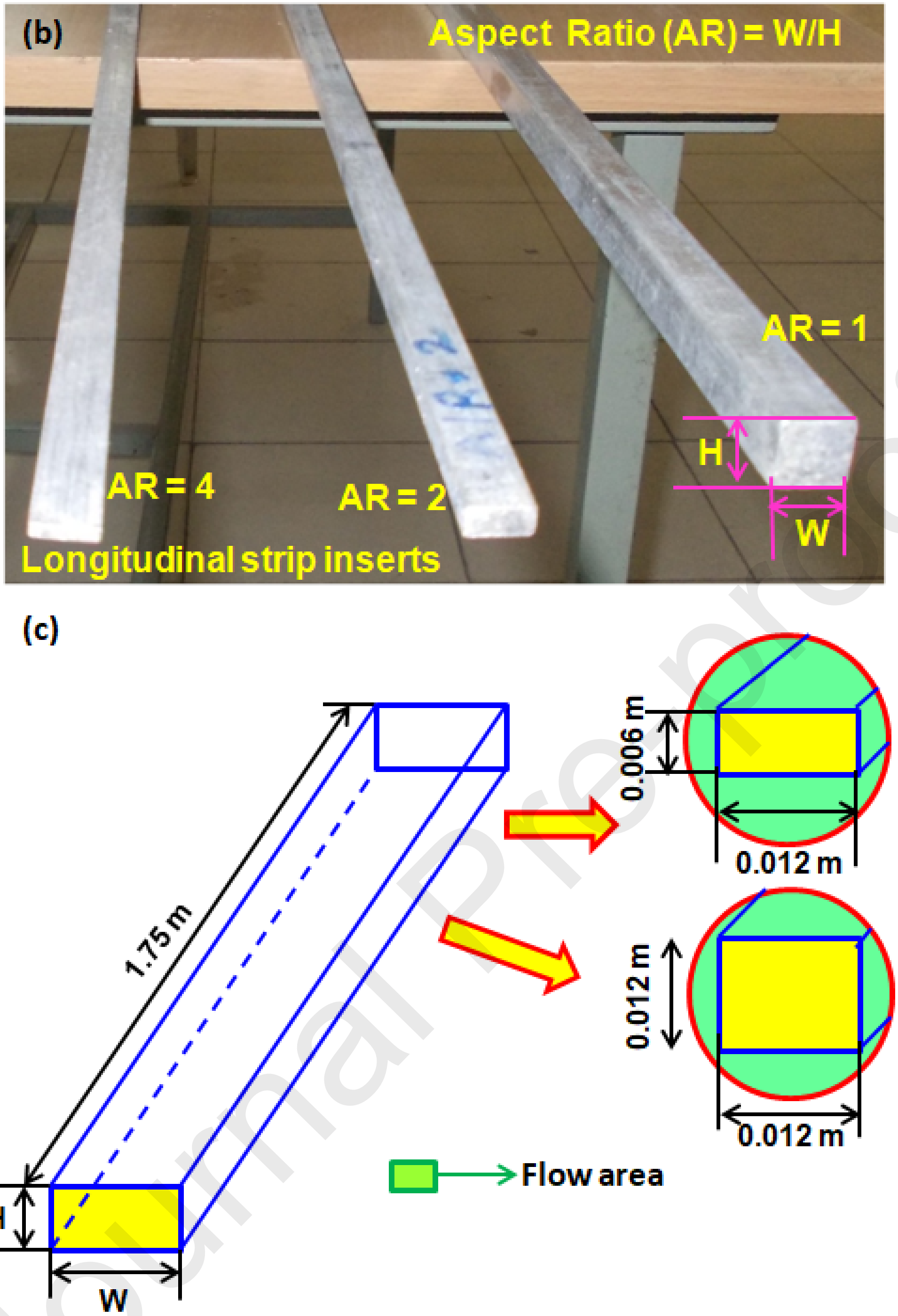


**Fig. 9(b)** Longitudinal strip inserts and (c) Cross sectional view of a longitudinal strip insert at section X-X.

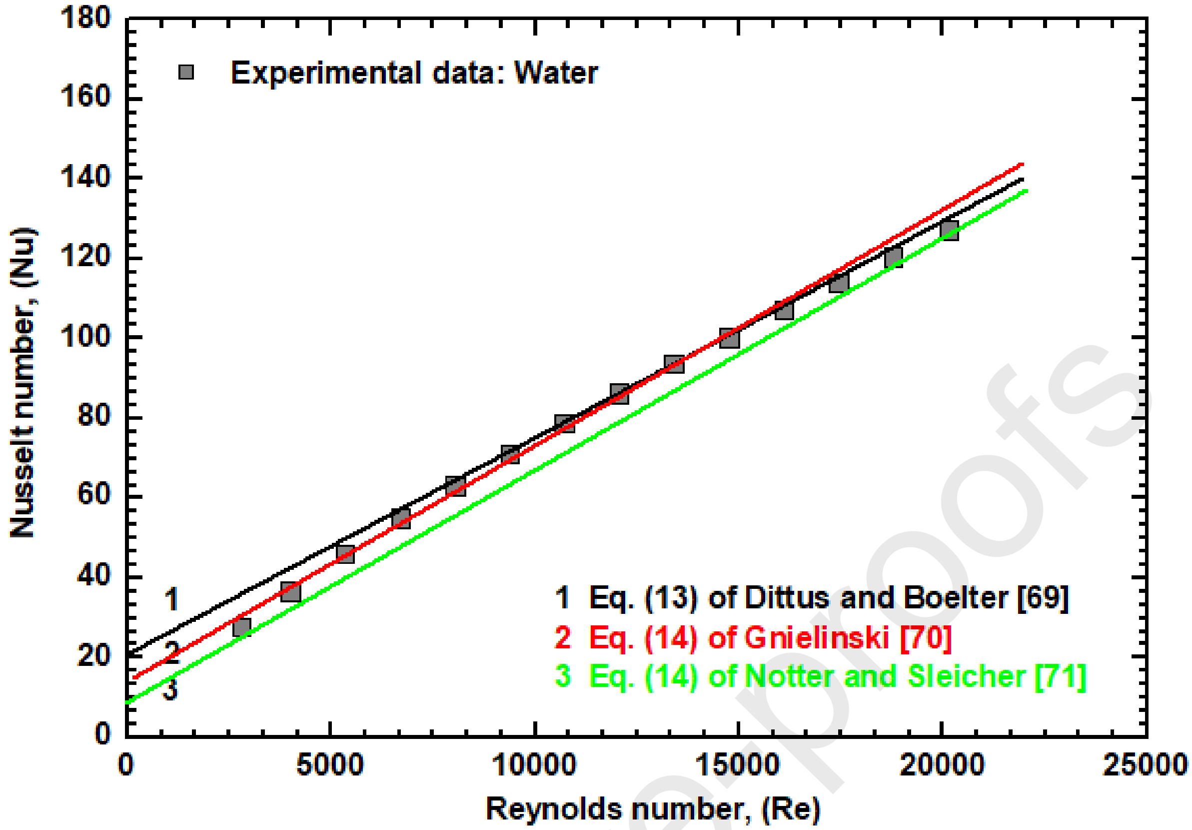


**Fig. 10** Validation of water Nusselt number against literature values

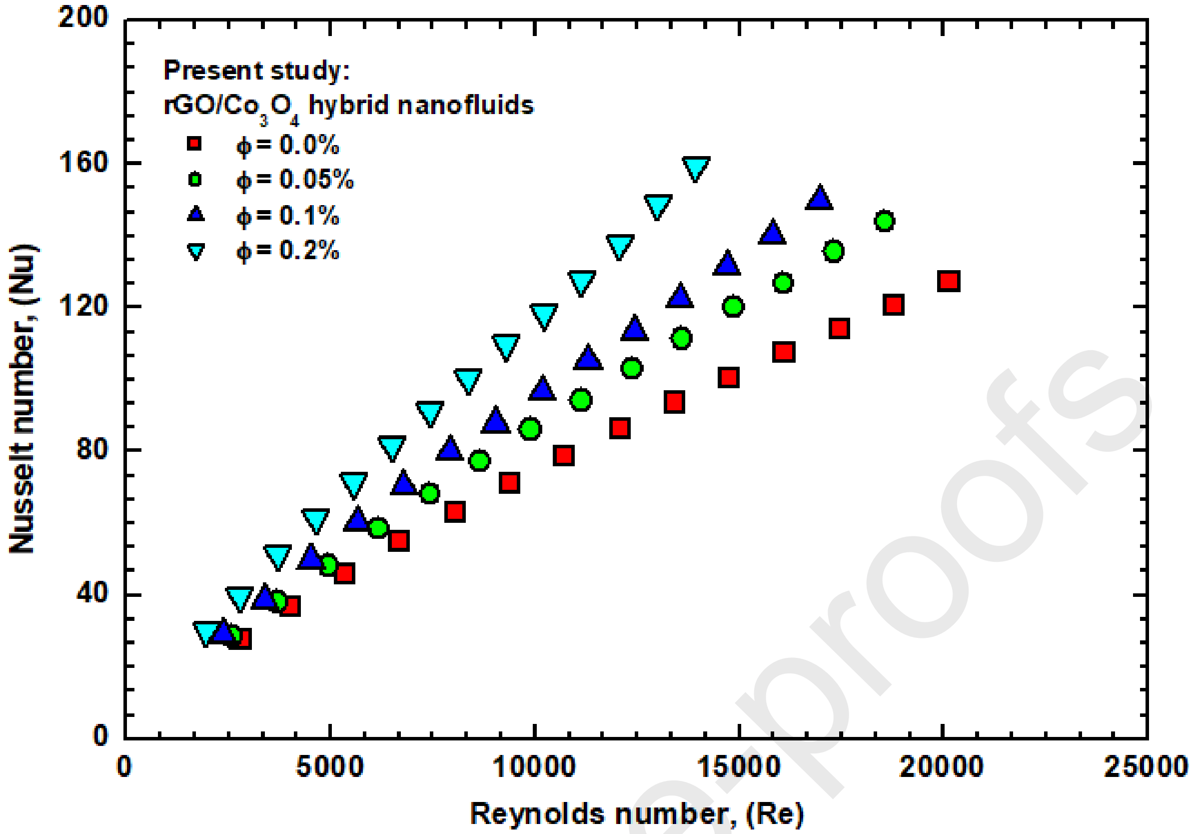


**Fig. 11** Nusselt number of rGO/$Co_3O_4$ nanofluids as a function of Reynolds number

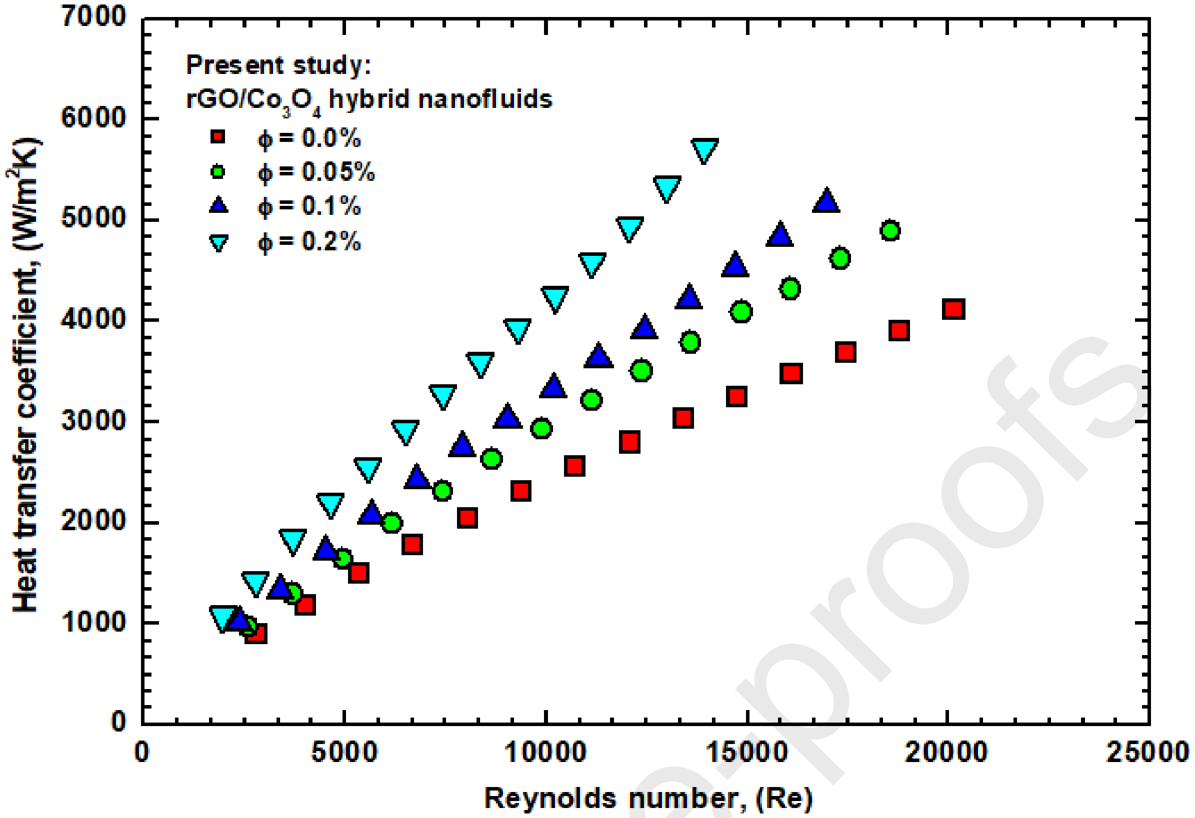


**Fig. 12** Heat transfer coefficient of rGO/$Co_3O_4$ nanofluids as a function of Reynolds number

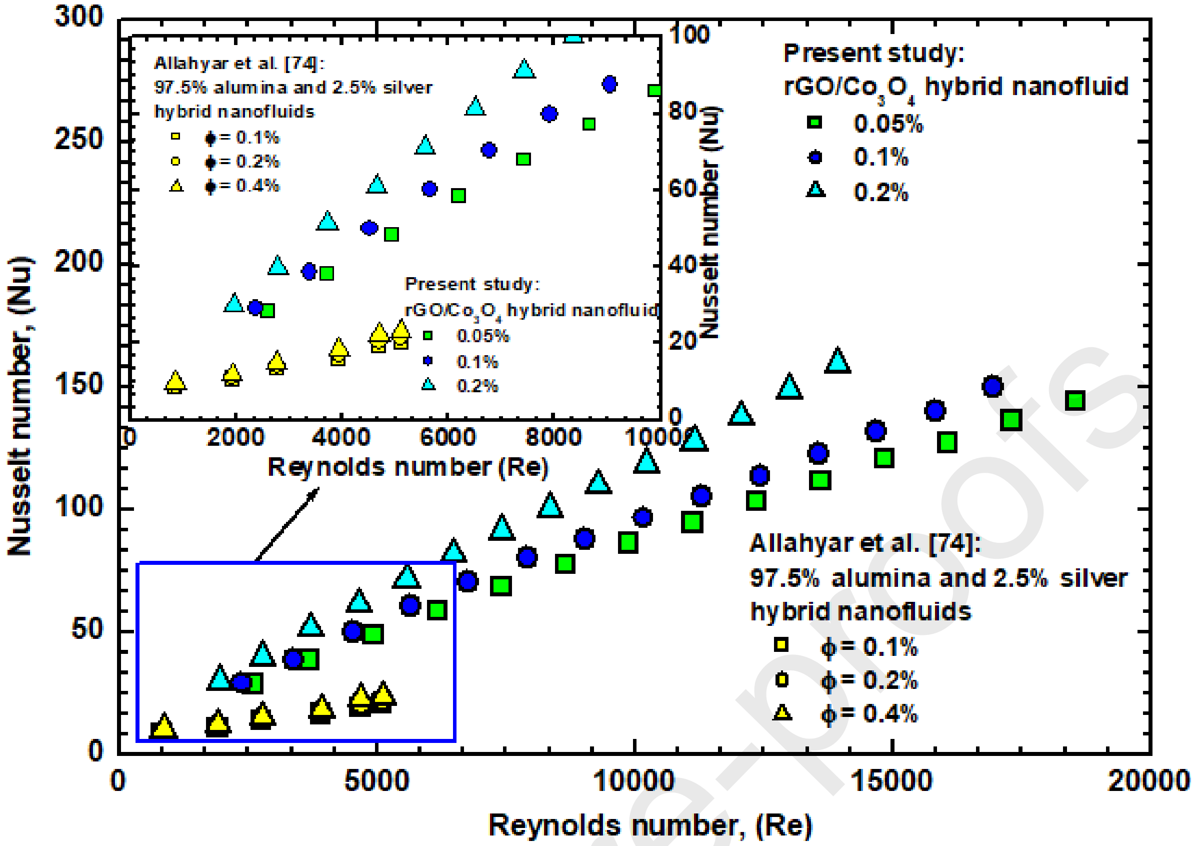


**Fig. 13** Comparison of the present rGO/$Co_3O_4$ nanofluids Nusselt number results with Allahyar et al. [74] data for 97.5% alumina and 2.5% silver hybrid nanofluids

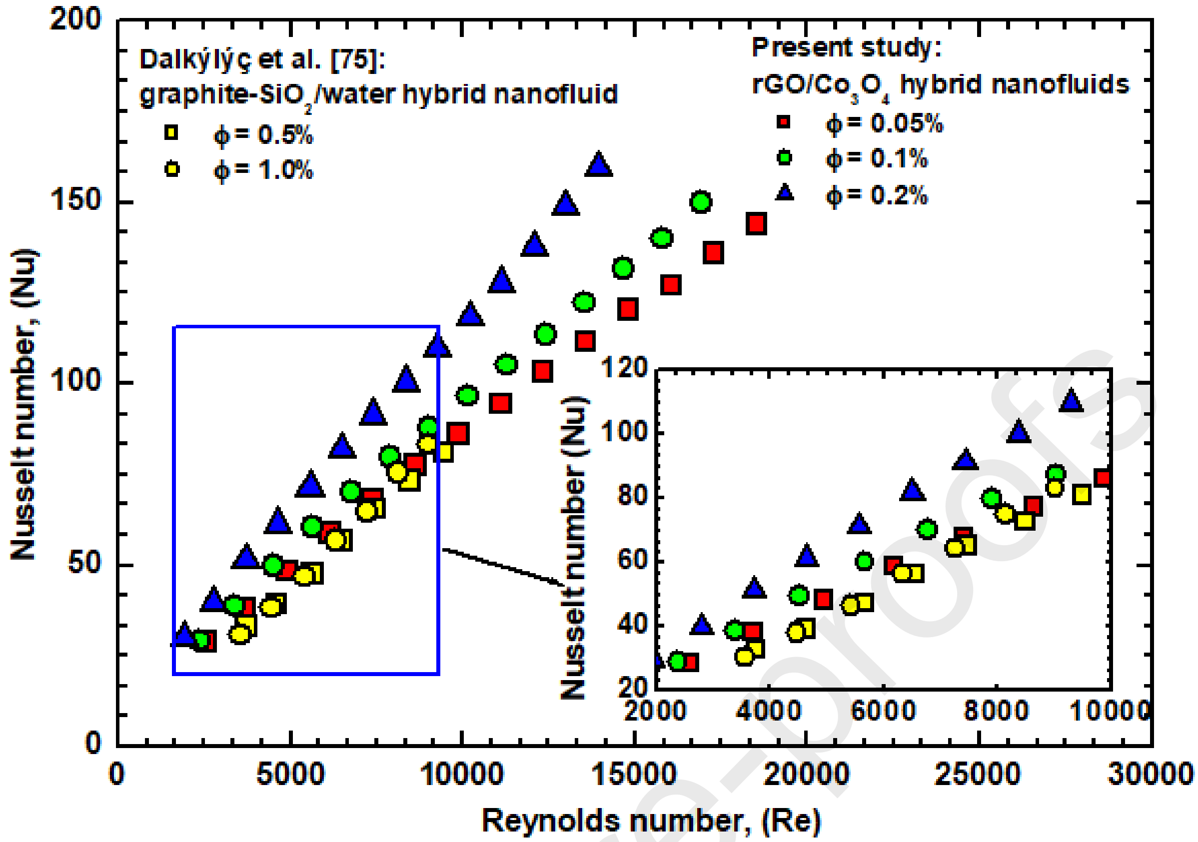


**Fig. 14** Comparison of present of rGO/$Co_3O_4$ nanofluids Nusselt number results with Dalkılıç et al. [75] data for graphite-$SiO_2$/water hybrid nanofluids

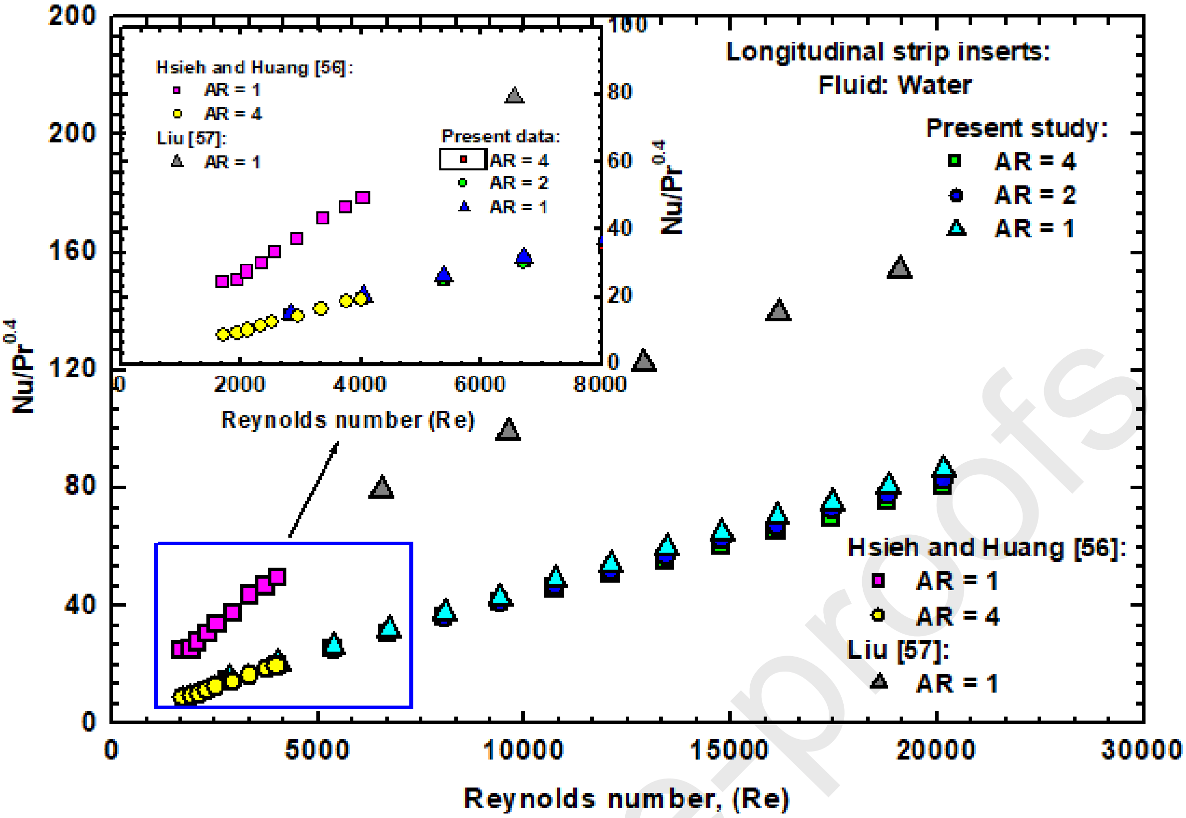


**Fig. 15** Validation of the results for water Nusselt number with longitudinal strip inserts with Hsieh and Huang [56] and Liu [57] data.

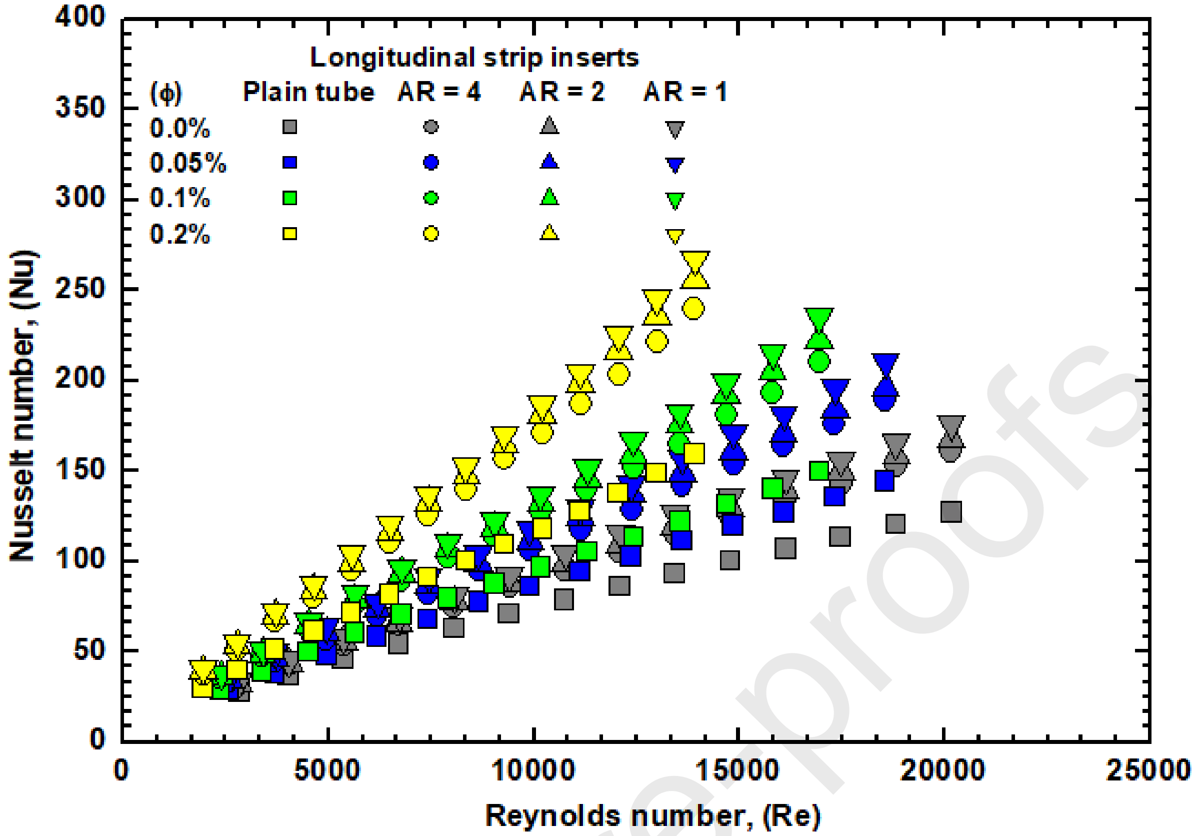


**Fig. 16** Nusselt number of rGO/$Co_3O_4$ nanofluids with longitudinal strip inserts as a function of Reynolds number

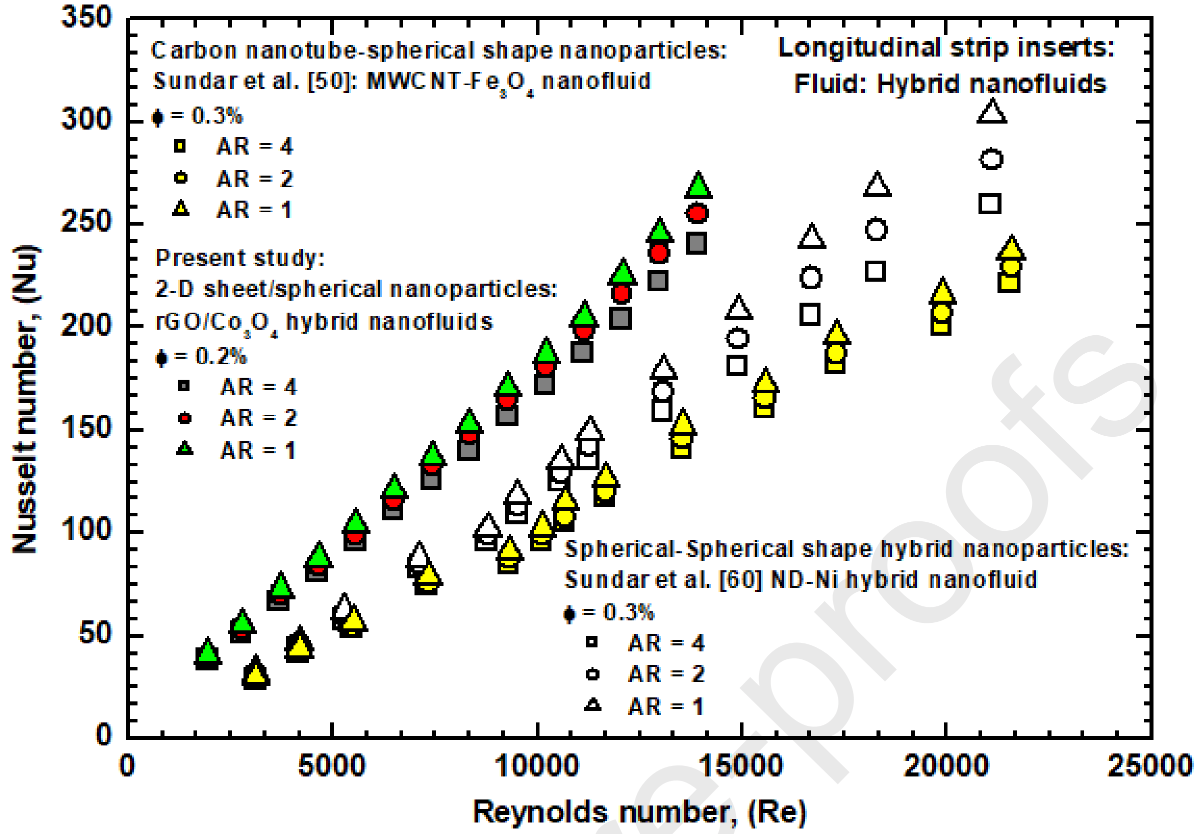


**Fig. 17** Comparison of the results for $rGO/Co_3O_4$ nanofluids Nusselt number with longitudinal strip inserts with the literature values

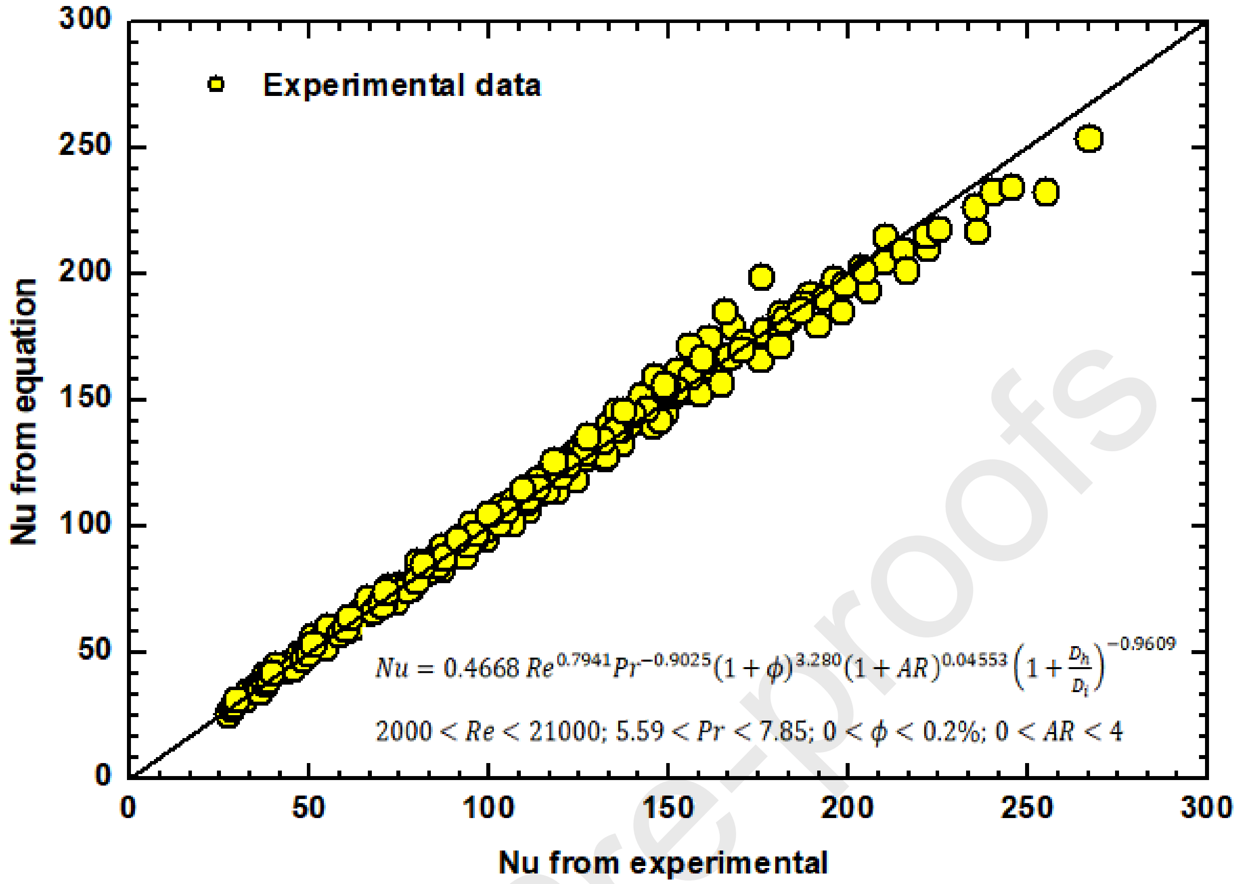


**Fig. 18** Validation of the proposed Nusselt number regression equation with the experimental data

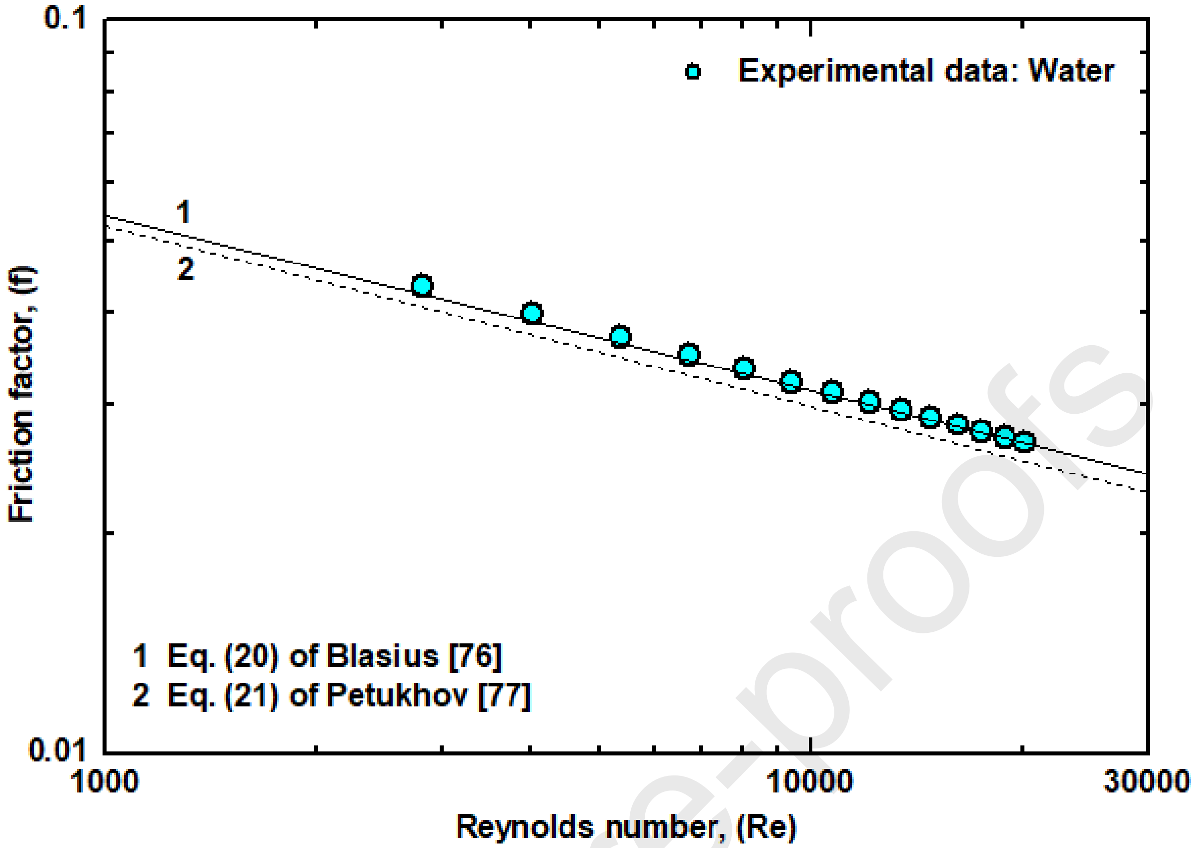


**Fig. 19** Comparison of water friction factor with literature values

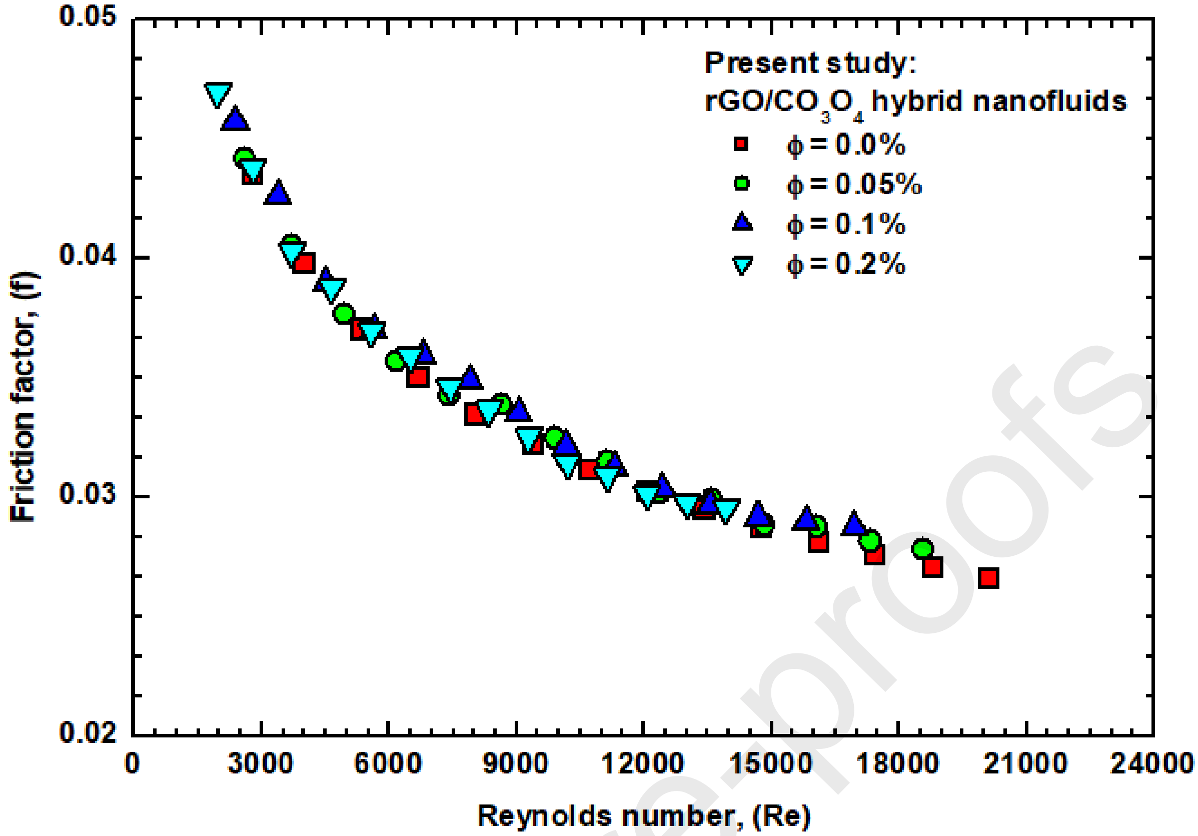


**Fig. 20** The friction factor of base fluid and rGO/$Co_3O_4$ nanofluids as a function of Reynolds number and particle concentration

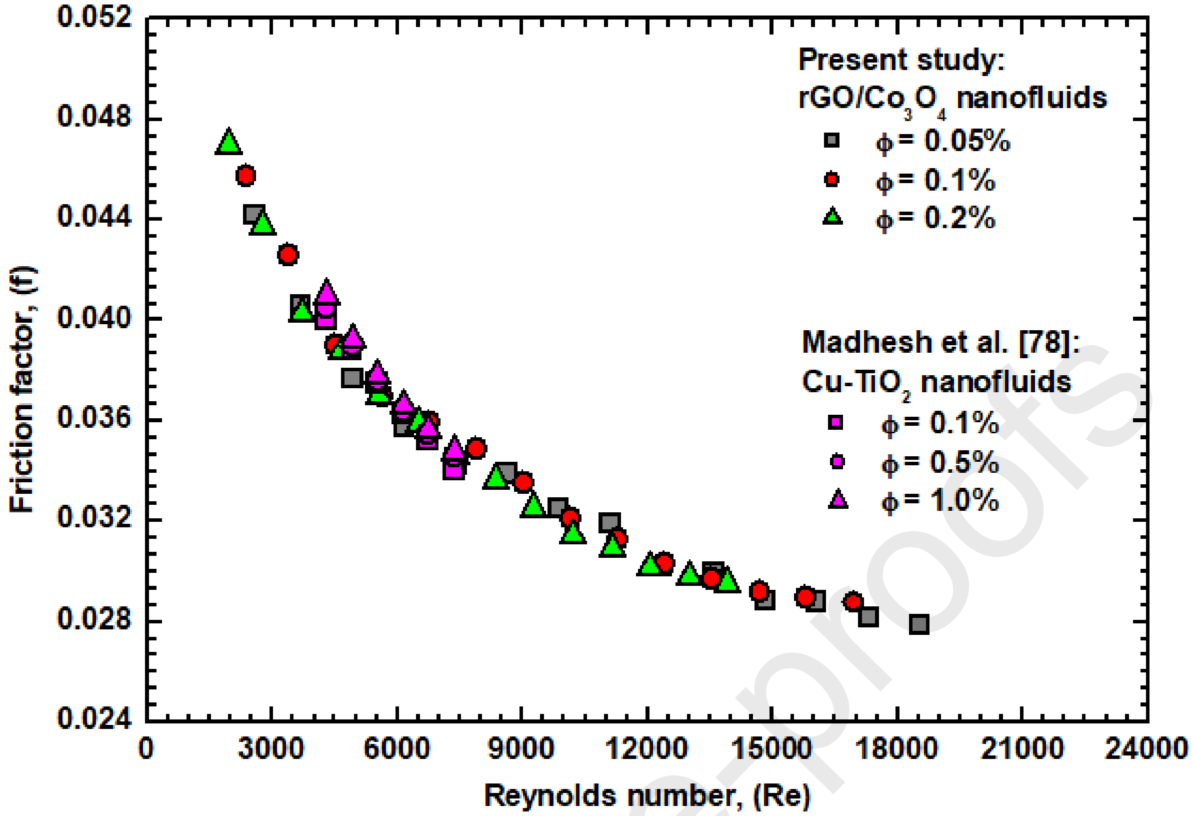


**Fig. 21** Comparison of friction factor values for rGO/$Co_3O_4$ hybrid nanofluid against the data of Madhesh et al. [68] for Cu-$TiO_2$ hybrid nanofluid

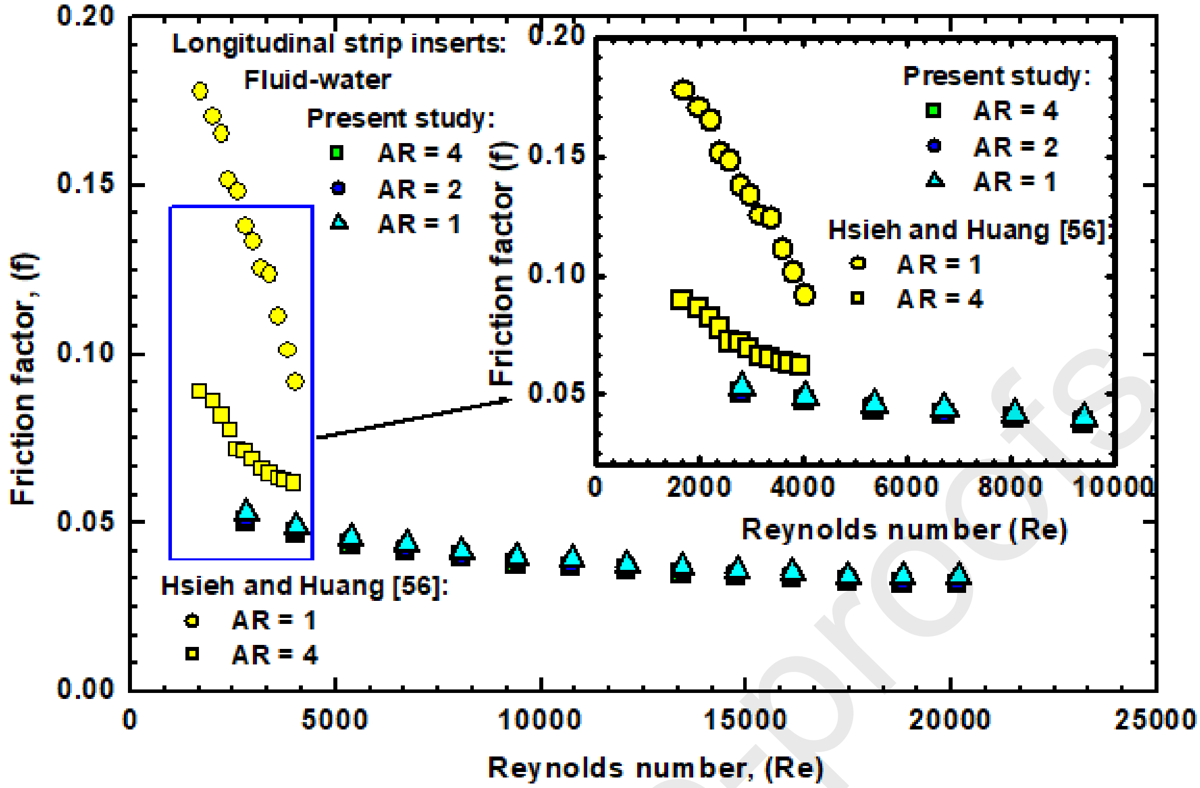


**Fig. 22** Comparison of friction factor values for water with longitudinal strip inserts with literature values

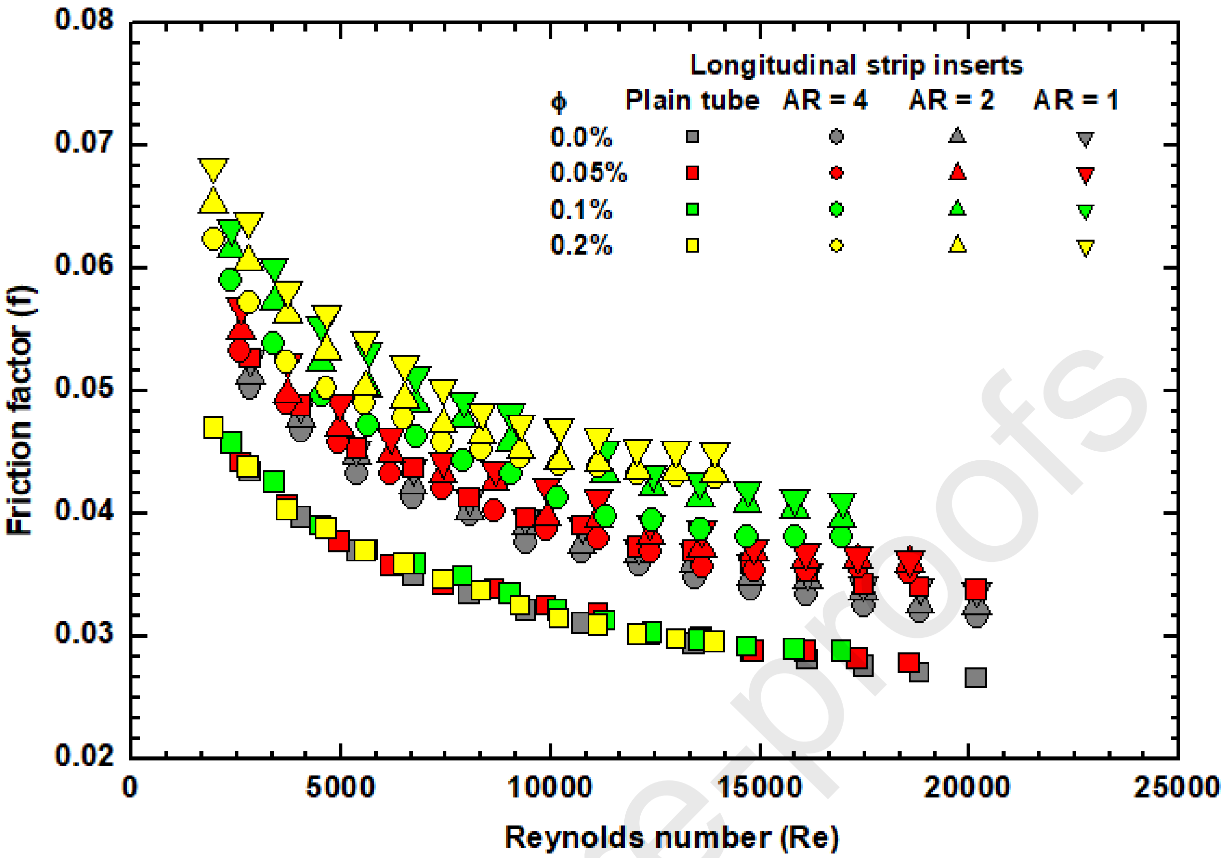


**Fig. 23** Friction factor of water and rGO/$Co_3O_4$ nanofluids with longitudinal strip inserts as a function of Reynolds number and particle loading

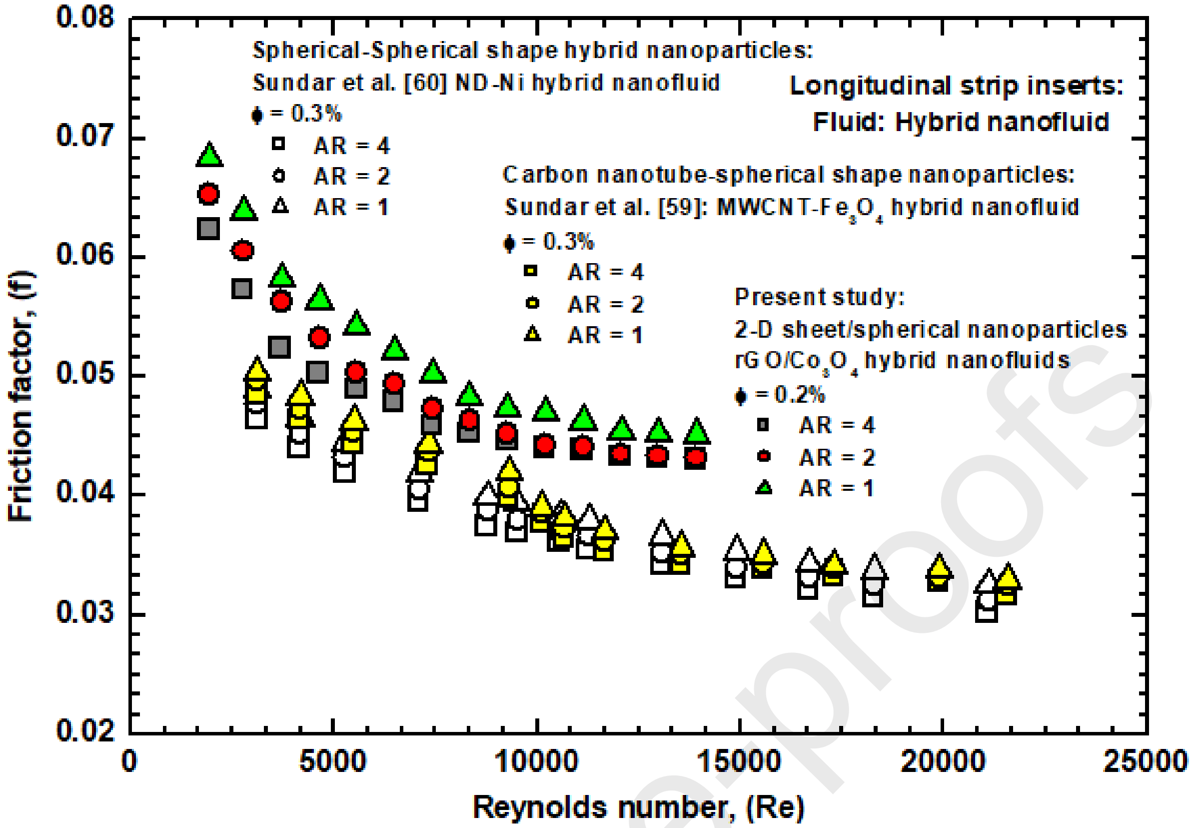


**Fig. 24** Validation of rGO/$Co_3O_4$ nanofluids friction factor with longitudinal strip inserts with literature values

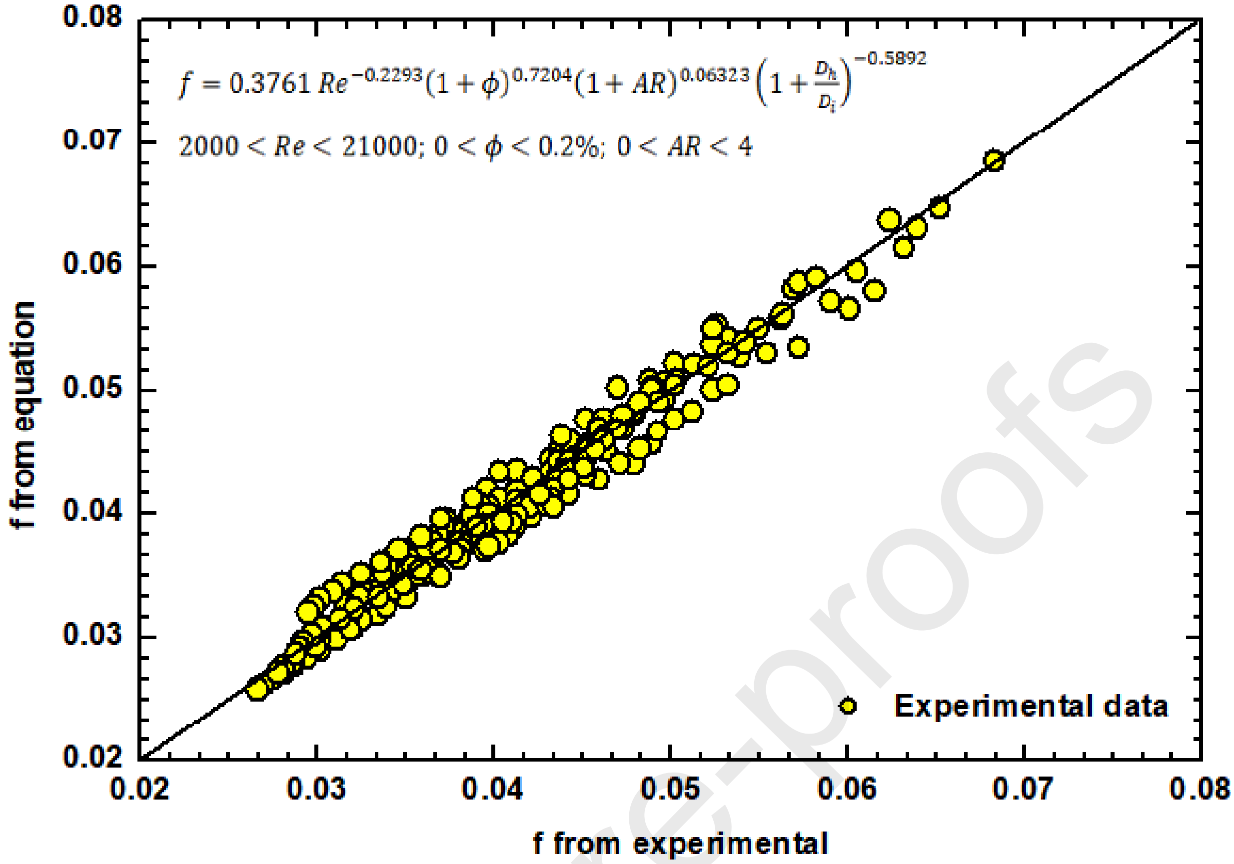


**Fig. 25** Validation of the proposed friction factor regression equation with the experimental data

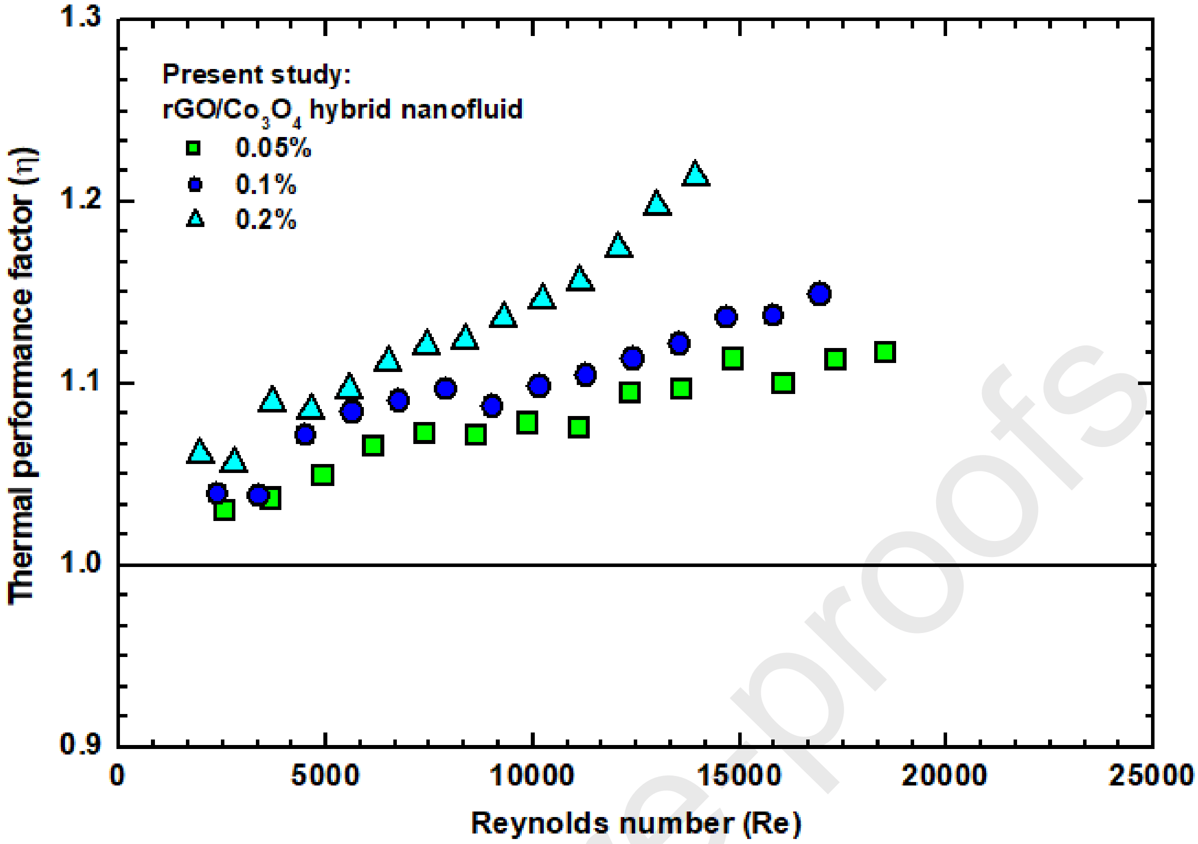


**Fig. 26** The thermal performance factor of rGO/$Co_3O_4$ nanofluids fordifferent values of Reynolds number

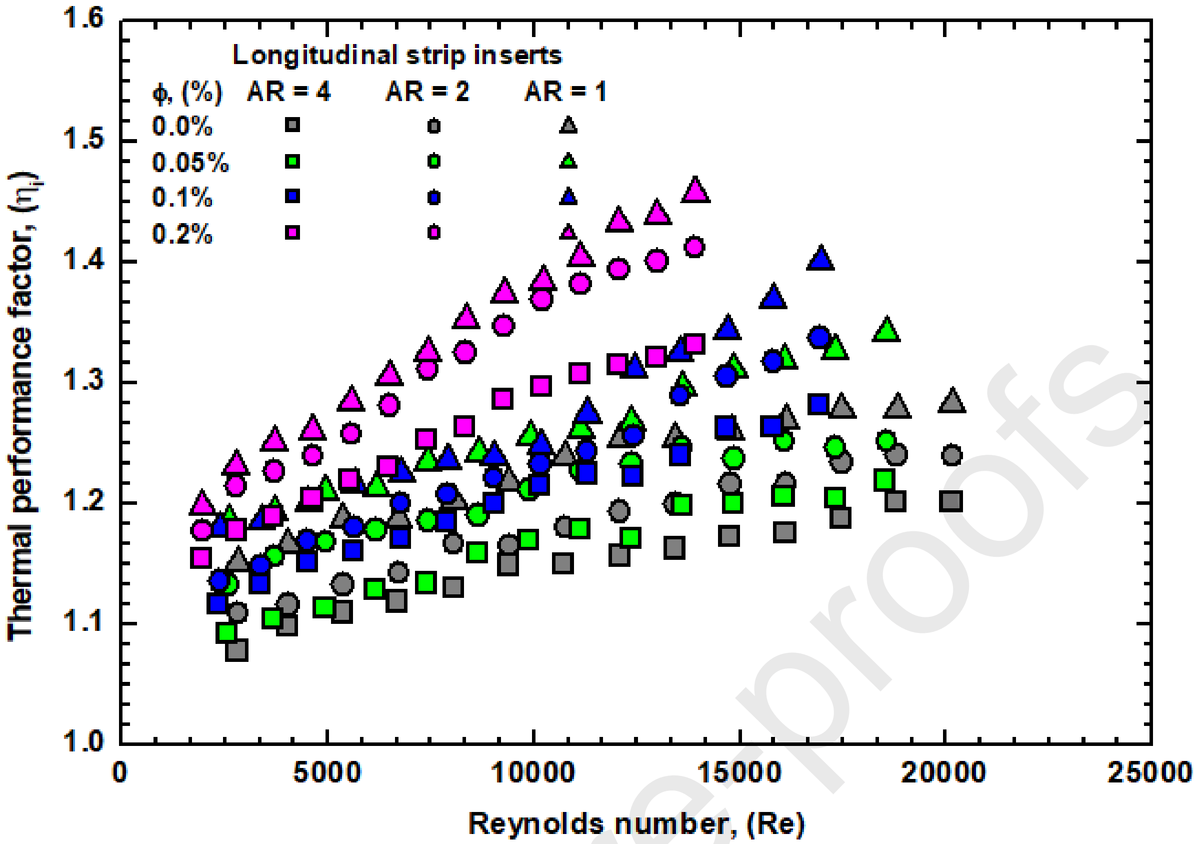


**Fig. 27** Thermal performance factor of water and rGO/$Co_3O_4$ nanofluids with longitudinal strip inserts for different values of Reynolds number



**Highlights**

**Combination of $Co_3O_4$ deposited rGO hybrid nanofluids and longitudinal strip inserts: Thermal properties, heat transfer, friction factor, and thermal performance evaluations**

(1) The water based hybrid nanofluids were prepared using rGO/$Co_3O_4$ nanomaterial.

(2) At, $\phi$ = 0.2 vol. % and Re = 13921, the Nusselt number is enhanced to 25.65% compared to water.

(3) At, $\phi$ = 0.2 vol. % and longitudinal strip AR = 1, the Nusselt number is further enhanced to 110.56% compared to water.

(4) Friction factor is increased to 11% and further increased to 69.8% at 0.2 vol. % with and without longitudinal strip insert AR = 1 compared to water.